Progress in Oceanography 77 (2008) 1–29

Contents lists available at ScienceDirect

Progress in Oceanography

journal homepage: www.elsevier.com/locate/pocean

Review

# Statistics from Lagrangian observations

J.H. LaCasce *

*Department of Geosciences, University of Oslo, P.O. Box 1022, Blindern, 0315 Oslo, Norway*

ARTICLE INFO

*Article history:*
Received 7 September 2007
Received in revised form 8 February 2008
Accepted 8 February 2008
Available online 29 February 2008

*Keywords:*
Lagrangian statistics
Floats
Drifters
Absolute and relative dispersion

ABSTRACT

We review statistical analyses of Lagrangian data from the ocean. These can be grouped into studies involving single particles and those with pairs or groups of particles. Single particle studies are the most common. The prevalent analysis involves binning velocities geographically to estimate the Eulerian means and lateral diffusivities. However single particle statistics have also been used to study Rossby wave propagation, the influence of bottom topography and eddy heat fluxes. Other studies have used stochastic models to simulate dispersion, calculated Lagrangian frequency spectra and examined the relation between Lagrangian and Eulerian integral scales. Studies involving pairs of particles are fewer, and the results are not well-established yet. There are indications that pair separations grow exponentially in time below the deformation radius, as is also the case in the stratosphere. The behavior at larger scales is less clear, indicating either a turbulent cascade or dispersion by the sheared large-scale circulation. In addition, three or more particles can be used to measure relative vorticity and divergence.



**Contents**



* Tel.: +47 228 55955; fax: +47 228 55269.
*E-mail address:* j.h.lacasce@geo.uio.no

0079-6611/$ - see front matter © 2008 Elsevier Ltd. All rights reserved.
doi:10.1016/j.pocean.2008.02.002

## 1. Introduction

Lagrangian instruments have been used to study large regions of both the atmosphere and ocean. Free-drifting instruments can cover large distances on their own, thereby reducing the need for (costly) direct sampling. The 483 balloons released in the 1970s during the EOLE experiment in the southern hemisphere stratosphere (Morel and Bandeen, 1973) offered an unparalleled glimpse of the synoptic winds there. However, because free-drifting instruments generally follow complex paths, the methods of analyzing the data are often different than with Eulerian data.

Hereafter we review a particular subset of Lagrangian analysis. In this, one recognizes that individual trajectories are largely unpredictable, so that a statistical description is preferable to a descriptive one. The primary goal is to discuss the different analyses which have been applied to ocean data. So we will focus on a few studies to illustrate the techniques, rather than discussing all related studies. A second goal is to see how the results reflect the underlying dynamics.

It is worth noting what this review does not cover. We will not present a survey of Lagrangian experiments (e.g. Davis, 1990; Rossby, 2007). Nor does the review cover dynamical systems theory, which concerns the flow structures which determine stirring (e.g. Wiggins, 2005). Dynamical systems theory thus far has been applied mostly to model data (e.g. Rogerson et al., 1999) and less to real data (Lozier et al., 1997; Kuznetsov et al., 2002). In addition, we will not consider Lagrangian data assimilation, even though this is currently an active area of research and is intimately linked with Lagrangian statistics. Recent reviews of assimilation are given by Bennett (2006), Molcard et al. (2007) and Chin et al. (2007).

First we examine briefly the various instruments used in ocean studies. Then we present a general introduction to the statistical measures, demonstrating how most of these relate to the drift and spreading of a cloud of tracer. Thereafter we examine specific analyses based on single particle trajectories, and then on multiple particles.

### 1.1. Instruments

Lagrangian instruments can be grouped into two categories: those that track surface currents and those that follow subsurface currents. The former are *drifters*. There are currently over 1200 drifters in all the major ocean basins as part of the World Drifter Program.[1] Drifters are comprised of a satellite-tracked transmitter and often, but not always, a subsurface drogue (e.g. Sybrandy and Niiler, 1992; Niiler et al., 1995). The drogue usually resembles a large kite or sock, and causes the transmitter to drift with the currents at the depth of the drogue, generally 5–50 m below the surface. The drifters are tracked with the Argos satellite system, which yields locations up to several times a day with a positional error of 150–1000 m. More recent models, designed for nearshore applications, can be tracked using GPS and cellular phones, and these can offer 100 m accuracy with fixes every 10 min (Ohlmann et al., 2005). A recent and useful overview on drifters is given by Lumpkin and Pazos (2007).

The subsurface instruments are *floats*.[2] Floats sink to a chosen depth (determined by the float's compressibility and ballasting) and follow currents there. Floats have also been modified to track density surfaces instead (e.g. Rossby et al., 1985), which is more in line with fluid parcel motion.

Because they are below the surface, floats cannot be tracked by satellite. Early floats such as the Swallow float (Swallow and Worthington, 1957) and the subsequent Sound Fixing and Ranging or "SOFAR" floats (Rossby and Webb, 1970) emitted low frequency sound pulses which were monitored by a network of microphones: the float positions were then determined by triangulation. Later, the inverse system (RAFOS, or "SOFAR" spelled backwards; Rossby et al., 1986) was developed, with subsurface sound sources and much smaller floats carrying microphones. These floats yield positions with an accuracy of roughly 1 km, from once to several times a day. Comprehensive surveys of float development were given by Gould (2005) and Rossby (2007).

A recent addition is the autonomous Lagrangian current explorer (ALACE) float (Davis et al., 1992) which drifts at a constant depth and rises to the surface periodically to be located by satellite. Because they are not tracked at depth, they do not require subsurface sound sources, which are expensive and limit the sampling region. A modified version of the float which measures density as it rises to the surface, the Profiling ALACE (PALACE) float, is now in wide use in the global ARGO program. However, because ALACE floats drift for days or weeks below the surface without being tracked, their temporal resolution is low. Because of this, we will not consider these floats in the subsequent discussions.

Lagrangian dispersion can also be gauged by tracking a passive tracer.[3] While lacking the temporal resolution of a continuously tracked float, tracer evolution can provide information about the drift speed and stirring. However, we will touch only briefly on tracer release experiments, focusing instead on continuously tracked instruments.

Lagrangian measurements have long been used for descriptive studies, following the pioneering work of John Swallow in the 1950s and 1960s (Swallow and Worthington, 1957; Swallow, 1971). Floats have been deployed in Gulf Stream rings (e.g. Cheney and Richardson, 1976) and Meddies (Richardson et al., 1989), as well as in Rossby waves (Price and Rossby, 1982). The trajectories yield information about both the paths and structures of the sampled features. Floats and drifters have also been used to infer the structure of large-scale currents like the Gulf Stream (Richardson, 1983; Fig. 1), the Norwegian-Atlantic Current (Poulain et al., 1996) and the Antarctic Circumpolar Current (Davis, 1998).

However, the ocean is highly variable, both spatially and temporally. Two particles deployed at the same location at different times (or two particles deployed simultaneously at slightly different locations) often follow very different paths. As such, it is not sensible to talk about the path of a single drifter because that path is almost certainly unique. As recognized early on by turbulence researchers (e.g. Batchelor, 1953), such indeterminacy necessitates a statistical or probabilistic description, inferred from ensembles of trajectories.

### 1.2. General notions

Lagrangian statistics involve averages of particle positions and/or velocities. The measures can be subdivided into those pertaining to single particles and those requiring two or more particles. Both single and multiple particle statistics are required for a full description of tracer evolution.

Consider a collection of particles, constituting a "cloud" of tracer. Of interest is how the cloud moves, and also how it spreads out. The mean drift concerns the displacement of the center of mass, for instance in the $x$-direction:

$$M_x(t) = \frac{1}{N}\sum_{i=1}^{N}[x_i(t) - x_i(0)]. \quad (1)$$

[1] The drifter data archive can be found at www.aoml.noaa.gov.

[2] B. Warren once asked me why "drifters" float while "floats" sink?

[3] A colorful example of this was when a container ship sank in the North Pacific in 1990 and released some 61,000 Nike sneakers. These were swept eastward and many landed along the Canadian and American west coasts. The distribution of groundings was used by C. Ebbesmeyer and colleagues to deduce the surface drift.

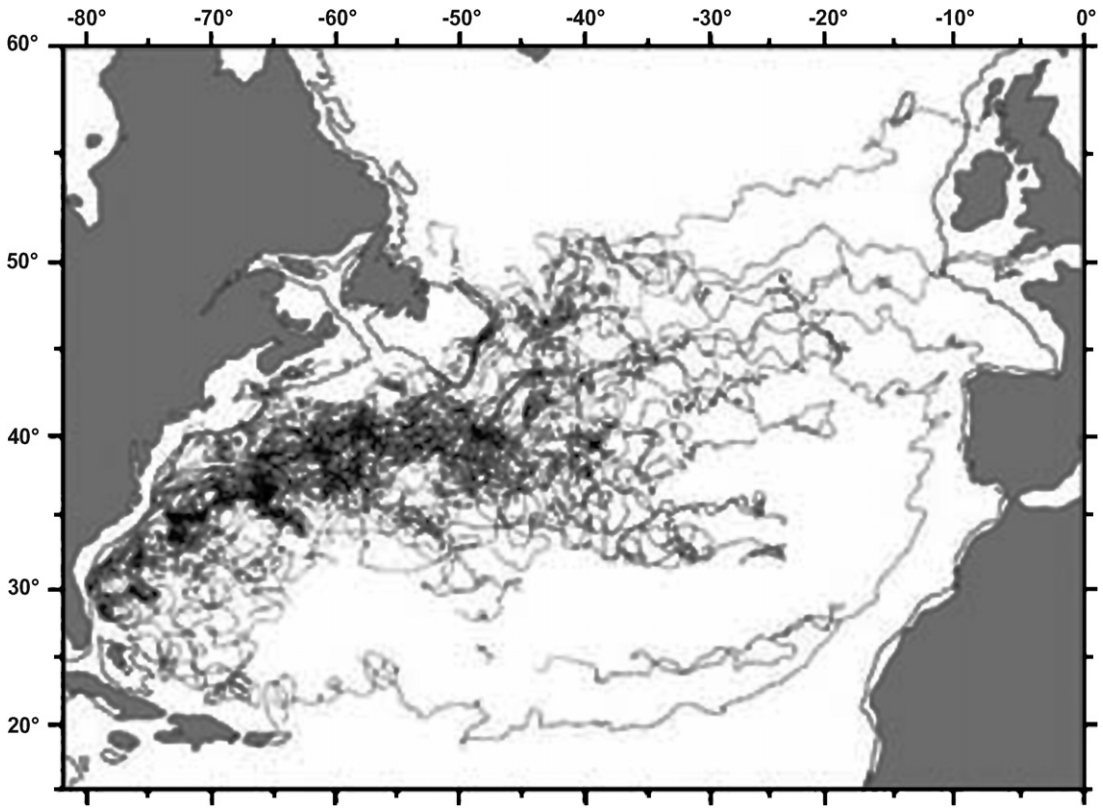


**Fig. 1.** Trajectories of surface drifters in the North Atlantic. From Richardson (1983), with permission.

This, the first moment of the displacements, is a single particle measure because it derives from individual trajectories.

The spread about the center of mass can be measured by the variance of the displacements, the second-order moment. This is[4]

$$D_x(t) = \frac{1}{N-1}\sum_{i=1}^{N}[x_i(t) - x_i(0) - M_x(t)]^2. \tag{2}$$

The variance is usually referred to as the "dispersion". We can rewrite the dispersion by expanding the RHS in (2). For example, consider three particles (and substituting $x_i$ for the displacement from the initial position):

$$\begin{aligned} D_x(t) &= \frac{1}{2}\left[\left(x_1 - \frac{x_1+x_2+x_3}{3}\right)^2 + \left(x_2 - \frac{x_1+x_2+x_3}{3}\right)^2 \right. \\ &\quad \left. + \left(x_3 - \frac{x_1+x_2+x_3}{3}\right)^2\right] \\ &= \frac{6}{18}\left[x_1^2 + x_2^2 + x_3^2 - x_1x_2 - x_1x_3 - x_2x_3\right] \\ &= \frac{1}{6}\left[(x_1-x_2)^2 + (x_1-x_3)^2 + (x_2-x_3)^2\right]. \end{aligned}$$

The analogous result for $N$ particles can be shown to be

$$D_x(t) = \frac{1}{2N(N-1)}\sum_{i\neq j}[x_i(t) - x_j(t)]^2, \tag{3}$$

where the sum is over all particle *pairs*.[5] Thus cloud dispersion is proportional to the mean square pair separation, known as the "relative dispersion". This equivalence reflects a general connection between two particle statistics and the concentration statistics of a scalar cloud (e.g. Batchelor, 1952a). It is a useful relation for experiments because cloud dispersion can be inferred from releasing pairs of particles rather than large clusters.

While the dispersion reflects the cloud's size, it is fairly insensitive to the cloud's distribution in space. Consider the two examples shown in Fig. 2. The upper left panel shows a group of particles undergoing a random walk (generated by a stochastic advection scheme; Section 2.3) while the upper right panel shows particles advected by a 2-D turbulent flow (Section 3.1.1). The cloud on the left is spreading uniformly while the one on the right is actually being drawn out into filaments. The result is two very different distributions.

A way to distinguish such cases is with the probability density function (PDF) of the displacements. The PDF, a normalized histogram, is of fundamental importance because all the moments (mean, dispersion, etc.) can be derived from it (Sections 2.1 and 3.1). Binning the $x$ displacements from the center of mass for the cloud at left in Fig. 2 yields the PDF in the lower left panel. This has a nearly Gaussian shape. The PDF for the turbulent flow on the other hand (lower right panel) has a peak near the origin and extended "tails". This reflects that most of the particles are near the origin while a few have been advected far away.

The dispersion measures the width of the PDF, and this is nearly identical for the two cases shown in Fig. 2. Where the distributions differ is in the higher-order moments. A frequently used one is the *kurtosis*, the fourth-order moment:

$$ku(x) \equiv \frac{\sum_i (x_i - M_x)^4}{\left[\sum_i (x_i - M_x)^2\right]^2}. \tag{4}$$

[4] We divide by $N-1$ to be consistent with the standard definition of the variance (one degree of freedom is lost determining the mean). Frequently $N$ is used instead.
[5] The additional factor of two corrects for counting pairs twice in the sum.

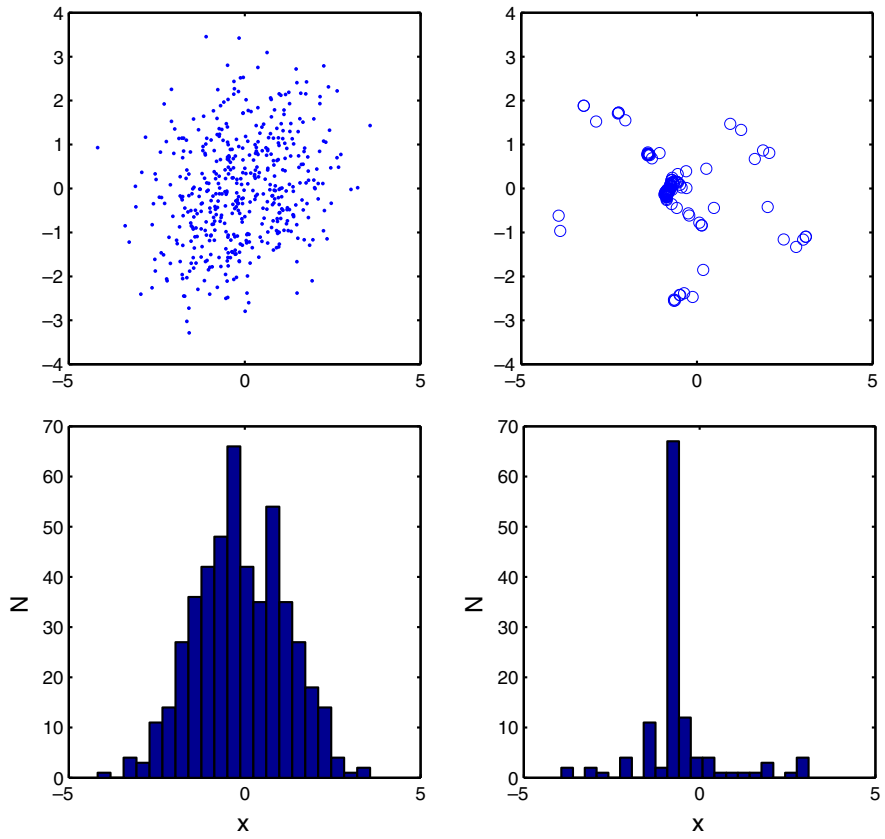


**Fig. 2.** Two examples of particle advection. The 484 particles in the upper left panel have been advected by a first-order stochastic routine (Section 2.3), while the 121 particles in the upper right panel were advected by a 2-D turbulent flow (Section 3.1.1). The lower panels show histograms of the *x*-displacements.

The kurtosis has a value of 3 for a Gaussian distribution. In the random walk example in Fig. 2 the kurtosis is 2.97, whereas in the turbulence case it is 6.62. The larger value reflects the extended tails.

Many of the measures discussed hereafter are variants on these fundamental quantities: the PDF and the moments (mean, dispersion and kurtosis), either for displacements or velocities. In addition, one can define similar quantities for both single particles and for pairs of particles. We consider single particle analyses first, and then continue with multiple particles thereafter.

## 2. Single particle statistics

A common starting point for single particle statistics is Taylor's (1921) seminal work on diffusion by continuous movements. A good summary was later given Batchelor and Townsend (1953). Davis (1991) discusses the application of such ideas to ocean data and also treats the problem of inhomogeneity. Bennett (2006) develops in detail the theoretical underpinnings. We also note the landmark study of Freeland et al. (1975), who applied many of these measures for the first time in analyzing SOFAR float data from the North Atlantic.

### 2.1. Theory

Consider a single fluid parcel, initially at $\mathbf{x} = \mathbf{x}_0$ at $t = t_0$. The probability that it arrives at $\mathbf{x}_1$ at time $t_1$ can be expressed by a single particle displacement PDF, $Q(x_1, t_1|x_0, t_0)$. If there is a group of particles initially, the probability of finding a particle at $(\mathbf{x}_1, t_1)$ is found by integrating over the initial positions:

$$P(x_1, t_1) = \int P(x_0, t_0) Q(x_1, t_1|x_0, t_0) \mathrm{d}x_0. \tag{5}$$

If the flow is statistically *homogeneous* (invariant to changes in location), then $Q$ is only a function of the displacement:

$$Q(x_1, t_1|x_0, t_0) = Q(x_1 - x_0, t_1, t_0) \equiv Q(X, t_1, t_0). \tag{6}$$

If the flow is also *stationary* (invariant to changes in time), then

$$Q(X, t_1, t_0) = Q(X, t_1 - t_0) \equiv Q(X, t). \tag{7}$$

The statistical moments (mean, variance, etc.) can all be derived from the PDF. The first moment is the mean displacement. For stationary, homogeneous flows, this is

$$\overline{X}(t) = \int X Q(X, t) \mathrm{d}X. \tag{8}$$

The second moment is the single particle or "absolute" dispersion:

$$\overline{X^2}(t) = \int X^2 Q(X, t) \mathrm{d}X. \tag{9}$$

Note the absolute dispersion is *not* the same as the cloud variance of Section 1.2. It is rather the variance of individual displacements relative to their starting positions, generally a very different quantity. With a translating cloud of particles, the absolute dispersion would reflect both the spread about the center of mass and the drift from the starting location. Thus the absolute dispersion is not Galilean invariant.

The time derivative of the single particle dispersion is the "absolute diffusivity":

$$\kappa(t) \equiv \frac{1}{2} \frac{\mathrm{d}}{\mathrm{d}t} \overline{X^2} = \overline{X(t) u(t)} = \int_0^t \overline{u(X, t) u(X, \tau)} \mathrm{d}\tau. \tag{10}$$

The diffusivity thus is the integral of the velocity autocorrelation. If the flow is stationary, then

$$\kappa(t) = v^2 \int_0^t R(\tau)\mathrm{d}\tau, \tag{11}$$

where $v^2$ is the velocity variance and $R$ the normalized velocity autocorrelation. Note that the velocity autocorrelation is the product of the velocity at time $t$ and the velocities at *previous* times. This reflects that the displacement at time $t$ is the integral of velocities up to $t$. However, for stationary flows the integral forward in time yields the same result, so that the $u(X,t)$ in the integral could be replaced by $u(X,0)$.

In addition, the dispersion can be written in terms of $R$:

$$\overline{X^2}(t) = 2v^2 \int_0^t (t-\tau)R(\tau)\mathrm{d}\tau. \tag{12}$$

Relation (12) can be used to deduce the dispersion under fairly general conditions. At early times, $R(\tau) \approx 1$ (following a Taylor expansion) and the dispersion thus grows quadratically in time:

$$\lim_{t\to 0} \overline{X^2}(t) = v^2 t^2. \tag{13}$$

At long times, we have

$$\lim_{t\to\infty} \overline{X^2}(t) = 2v^2 t \int_0^\infty R(\tau)\mathrm{d}\tau - 2v^2 \int_0^\infty \tau R(\tau)\mathrm{d}\tau. \tag{14}$$

If the integrals in (14) converge, the dispersion grows *linearly* in time. Thus the diffusivity is constant, implying the advection can be represented as a diffusive process, with the diffusivity determined as above. Of course this is only true in a statistical sense; individual events could vary greatly. But a large ensemble of such events would exhibit diffusive spreading.

The linear dependence fails under certain conditions, for instance if there is a long-time correlation in the velocity field or if the spread of particles is restricted, as in an enclosed basin (Artale et al., 1997). In addition, one may observe *anomalous* dispersion, or dispersion with a power law dependence different than $t^1$ or $t^2$ (e.g. Young, 1999; Ferrari et al., 2001) between the initial and final asymptotic limits. Anomalous dispersion has been observed in both numerical and laboratory experiments (e.g. Solomon et al., 1993), but has been more difficult to resolve in oceanic flows.

Other quantities can also be derived from the velocity correlation. The integral of the normalized autocorrelation is the "integral time":

$$T_L \equiv \int_0^\infty R(\tau)\mathrm{d}\tau. \tag{15}$$

This estimates the time scale over which the Lagrangian velocities are correlated and is a basic indicator of Lagrangian predictability. The diffusivity is thus the product of the velocity variance and the Lagrangian time scale, from (11). The Fourier transform of the velocity autocorrelation is the Lagrangian frequency spectrum (Taylor, 1938; Kampé de Fériet, 1939):

$$L(\omega) = 2v^2 \int_0^\infty R(\tau)\cos(2\pi\omega\tau)\mathrm{d}\tau. \tag{16}$$

Thus we have that

$$L(0) = 2v^2 T_L = 2\kappa. \tag{17}$$

So the absolute diffusivity is determined by the *lowest* frequency motion (e.g. Davis, 1982).

### 2.2. Advection–diffusion

This last point implies that a mean flow will alter the diffusivity. Indeed, a constant mean will cause the absolute dispersion to increase quadratically in time, and thus the diffusivity to increase linearly in time. So one should remove the mean velocities prior to calculating the diffusivity. In the ocean this is complicated by the fact that the means vary with location and depth.

Such issues have been considered in depth by Davis in a series of articles (Davis, 1982, 1983, 1987, 1991). His methodology is widely used in ocean data analysis. The general notion is that velocities from different floats and times are averaged over defined geographical regions to estimate the Eulerian mean velocities. These are then subtracted from the observed velocities, leaving the mean and "residual" velocities:

$$U(x,y,z) \equiv \langle u(x,y,z)\rangle, \quad u'(x,y,z,t) \equiv u(x,y,z,t) - U(x,y,z).$$

The brackets here represent the ensemble average in the selected geographical region. The diffusivity is then estimated from the residual velocities. The underlying assumption is that the mean and residual velocities are well separated in time, so that the averaging properly resolves the mean.

The means and diffusivities can then be used to write a transport equation for a passive tracer, $C$:

$$\frac{\partial}{\partial t}C + U\cdot\nabla C = -\nabla\cdot\langle u'C'\rangle \equiv \nabla\cdot(\kappa\nabla C). \tag{18}$$

This in turn could be used to predict the spread of pollutants, nutrients or salinity in the sampled region.[6] The equation is essentially the "semi-empirical" equation for turbulent diffusion (Monin and Yaglom, 2007; Bennett, 2006).

This procedure thus uses Lagrangian data to estimate the Eulerian mean velocity. The diffusivity on the other hand is a mixed Eulerian–Lagrangian statistic, as it involves the velocity residual at a fixed location. Note that representing the eddy flux as a diffusion assumes that the diffusivity actually exists.

An advantage of Eq. (18) is that all the required terms can be calculated from single particle statistics. We begin with the mean, and then consider the diffusivity.

#### 2.2.1. Mean flow

As noted, the advective–diffusive formalism assumes a separation in time scales or, equivalently, a gap in the velocity frequency spectrum (16). All indications are that no such gap exists, either in the atmosphere or ocean (e.g. Gage and Nastrom, 1986; Zang and Wunsch, 2001). We make the assumption nevertheless, for utility's sake. But what time scale should be used to separate the mean from the residuals? A practical choice is the length of the float experiment in question (Davis, 1991), which might be a year or two.

As noted, the mean is calculated by averaging velocities of particles passing through selected geographical bins. We assume the statistics are stationary, i.e. that the variability in the bin is not changing over the duration of the experiment. Thus while we anticipate variations in space, we neglect them in time. In addition, the means pertain to the vertical position (or isopycnal) occupied by the floats in the experiment.

Richardson (1983) estimated mean surface velocities from drifters by averaging the data shown in Fig. 1. Owens (1991) mapped the subsurface mean velocities in the western North Atlantic using SOFAR float data. Shown in Fig. 3 is a more recent estimate, deriving from the surface drifters present in the North Atlantic during the 1990s (Fratantoni, 2001). The Gulf Stream is seen separating from the coast off Cape Hatteras and then flowing eastward. The current splits, with part proceeding north and the rest continuing eastward. The North Brazil Current is also seen, retroflecting north of the equator to feed the North Equatorial Counter Current, as is the intensified boundary currents in the Caribbean and off Greenland.

[6] An alternate version, preferred by Davis, includes a second-order time derivative for the tracer field. This allows for wave propagation, thus avoiding the issue of tracer signals propagating infinitely fast as in the diffusion equation (Davis, pers. comm.).

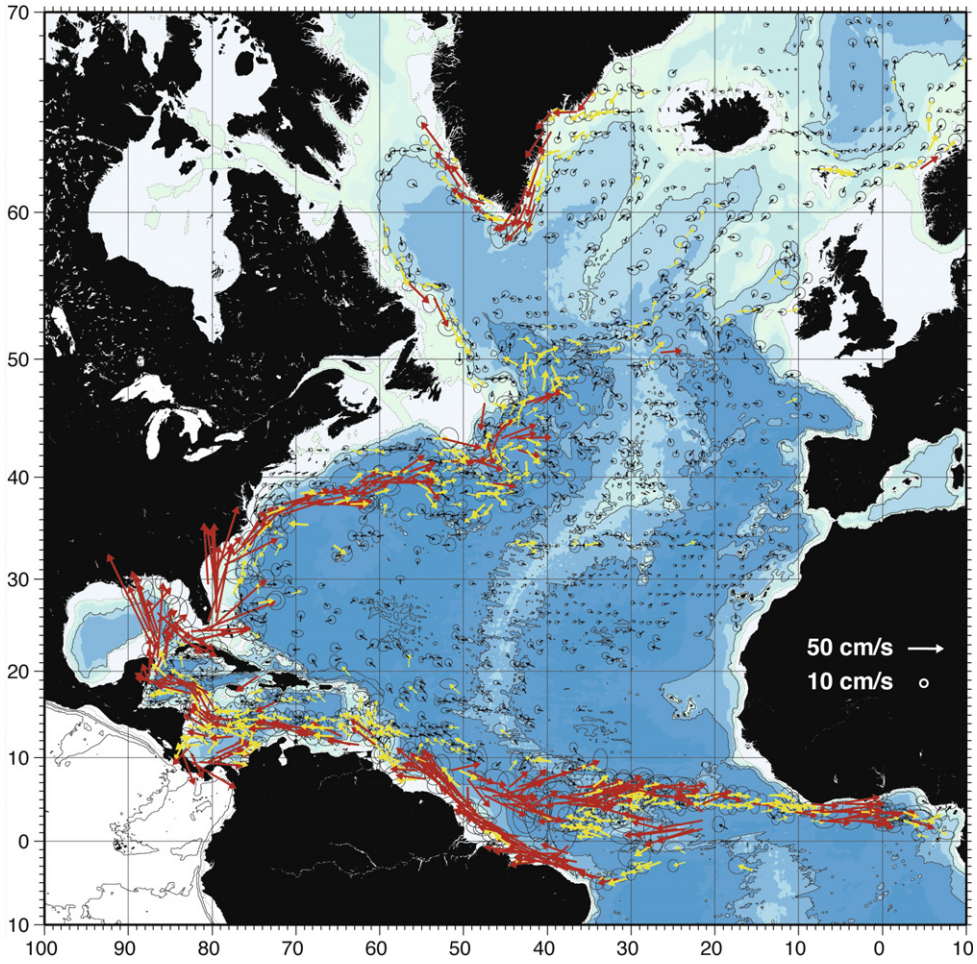


**Fig. 3.** Mean velocities obtained from averaging velocities from surface drifters in the North Atlantic from the 1990s. The means are only plotted at points where they are significantly different from zero. From Fratantoni (2001), with permission.

Another example, from the Nordic Seas, is shown in Fig. 4. This figure, derived from surface drifter data by Jakobsen et al. (2003), captures the North Atlantic Current as it crosses the basin and enters the Nordic Seas (e.g. Mauritzen, 1996). The Greenland Current is also seen, rounding the southern tip of Greenland and proceeding into the Labrador Sea.

While results like these are compelling, there are pitfalls with the binning method. First, the significance of the mean in a given bin depends on the number of drifters which have been through. In many published analyses, the means are only plotted for bins with more than some minimum number of velocity realizations. Alternately, one could show only those means which are significantly different than zero; this is what Fratantoni (2001) did in Fig. 2. Indeed, this is why the central North Atlantic appears blank in the figure, because the average velocities there aren't significantly different from zero.

The second concerns the size of the bins. Just as there is no spectral gap in the velocity frequency spectrum, neither is there a gap in the wavenumber spectrum. So the chosen bin size affects the horizontal scale of the mean flow. Choosing too large bins yields an overly smooth mean while using too small bins risks having the means biased by eddies. The Gulf Stream is typically problematic in this regard: it spans a large region but has a relatively narrow core. In addition, it meanders and so will occupy different bins (e.g. Zhang et al., 2001).

A third issue is that floats tend to drift up the gradient of eddy kinetic energy. Consider the advective-diffusion equation (18) without a mean flow:

$$\frac{\partial}{\partial t}C = \nabla\cdot(\kappa\nabla C), \tag{19}$$

where the diffusivity, $\kappa$, varies in space. Multiplying by $\vec{x}$ and integrating in space yields an equation for the tracer's center of mass:

$$\frac{\mathrm{d}}{\mathrm{d}t}\frac{\int \vec{x}C\mathrm{d}V}{\int C\mathrm{d}V} = \frac{\int C\nabla\kappa\mathrm{d}V}{\int C\mathrm{d}V}, \tag{20}$$

following integration by parts (Freeland et al., 1975). Thus if the eddy energy varies in space, the center of mass will migrate, towards the more energetic regions.

Furthermore the means are affected by having uneven data coverage. If all the floats in an experiment are deployed on the west side of a basin, dispersion will produce an apparent drift to the east without any mean flow. This "array bias" can in principle be corrected (Davis, 1991).

Several improvements to the method have also been explored. One, objective analysis (Bretherton et al., 1976), uses the bin estimates to derive the mean via a variational calculation (e.g. Davis, 1998; Lavender et al., 2000; Gille, 2003). Another approach is to fit the binned velocities with cubic splines (Bauer et al., 1998). In this, the "roughness parameter", which determines the spatial resolution of the mean, is chosen to minimize the low frequency energy in the eddy field. Both techniques yield smoother means, and this in turn affects the residual velocities.

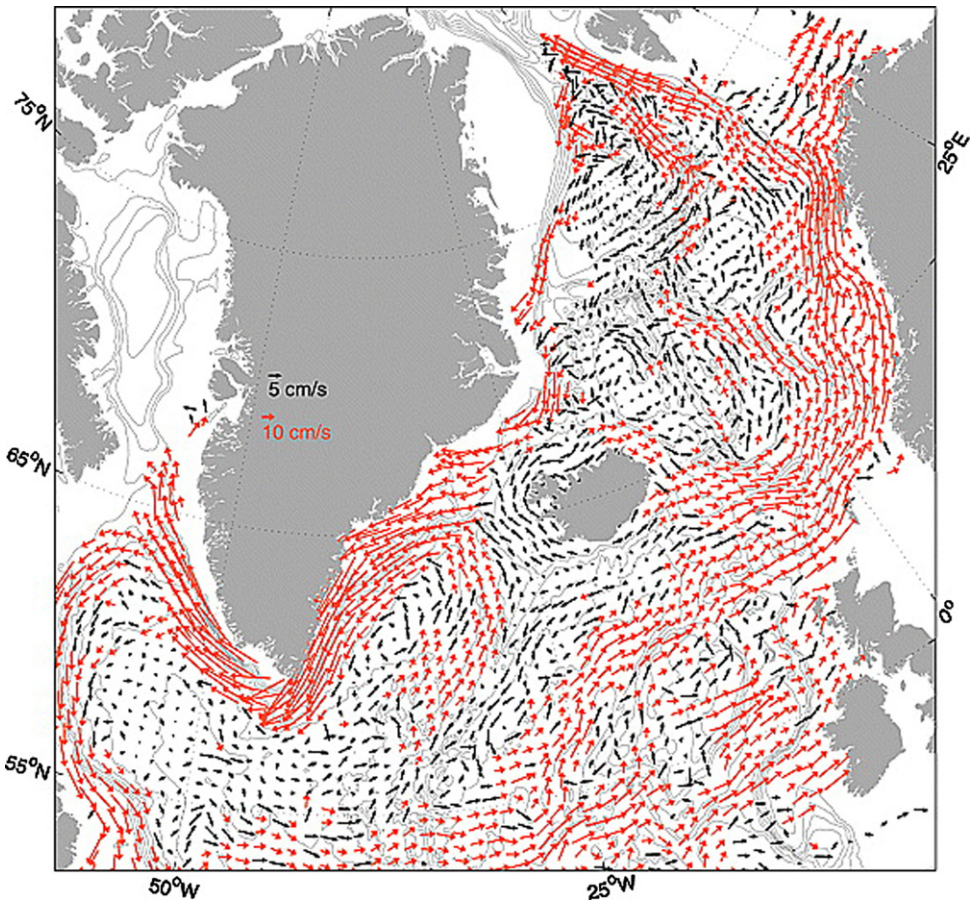


**Fig. 4.** Mean velocities derived from surface drifters in the northern North Atlantic and Nordic Seas. From Jakobsen et al. (2003), with permission.

*2.2.2. Diffusivity*

Similar issues affect calculating diffusivities. Floats typically visit different regions during their lifetime, and thus it is not sensible to integrate the autocorrelation in (10) to $t = \infty$. And because the "mean flow" is not truly stationary, some fraction of the low frequency variance will always remain in the residual velocity, directly affecting the diffusivities. As with the means, practical choices are required.

The diffusivity can be defined (Davis, 1991):

$$\kappa_{jk}(\mathbf{x}, t) = \int_{-t}^{0} \langle u'_j(t_0|\mathbf{x}, t_0) u'_k(t_0 + \tau|\mathbf{x}, t_0)\rangle \mathrm{d}\tau, \tag{21}$$

where the residual velocities are

$$u'(t_0) = u(t_0) - U(\mathbf{x}).$$

The diffusivity is a tensor, with possibly non-zero off-diagonal elements. The latter occur when the horizontal velocities are correlated, as under rotation (Section 2.3). The diffusivity can be divided into symmetric and asymmetric parts, and only the former contributes to the tracer diffusion.

The diffusivity can alternately be written in terms of the displacement:

$$\kappa_{jk}(\mathbf{x}, t) = -\langle u'_j(t_0|\mathbf{x}, t_0) d'_k(t_0 - t|\mathbf{x}, t_0)\rangle, \tag{22}$$

where the residual *displacement* is defined:

$$d'(t) = d(t) - d_m(\mathbf{x}, t).$$

Here $d_m(\mathbf{x}, t)$ is the displacement due to the mean flow. The integral in (21) and the displacement in (22) are defined backwards from the time, $t_0$, reflecting that the displacement of the particle arriving at $\mathbf{x}$ at $t = t_0$ is the integral over the previous velocities. Generally the integral in (21) is only evaluated up to a chosen time, for instance a typical time the float stays in a region or bin. This might be several times the integral time scale, $T_L$.[7]

Zhurbas and Oh (2004) used the method to map the diffusivity for the surface North Atlantic (Fig. 5). The Gulf Stream is a region of increased dispersion, as are the Caribbean, the Equator, the Falkland Current and the Agulhas retroflection. These are among the most energetic regions in the Atlantic, and the large variances account in large part for the high diffusivities.

There are several additional points. Davis's construct assumes that the residual velocities have a nearly Gaussian distribution. This has been tested in several locations and found to be approximately true (Section 2.4).

Second, diffusivity estimates can be affected by non-uniform float coverage, as with the means. The drift from regions with high float densities to those with low densities can yield a false impression of a diffusivity gradient. Correcting for this is not straightforward (Davis, 1991), so one must be wary of estimates from very non-uniform deployments.

In addition, the way the mean is calculated affects the diffusivities. This is particularly important in regions with significant lateral shear (e.g. Zhang et al., 2001). A specific example is shown in Fig. 6, from drifter data from the Pacific. The authors found that subtracting either a constant mean or a mean derived from binned velocities produced diffusivities which increased monotonically in time. However, when the mean was calculated by fitting the aver-

[7] Taken in reverse, one could define the minimum bin size as the rms distance floats spread from a central point over several integral times. Such an approach would help prevent integrating eddies into the mean.

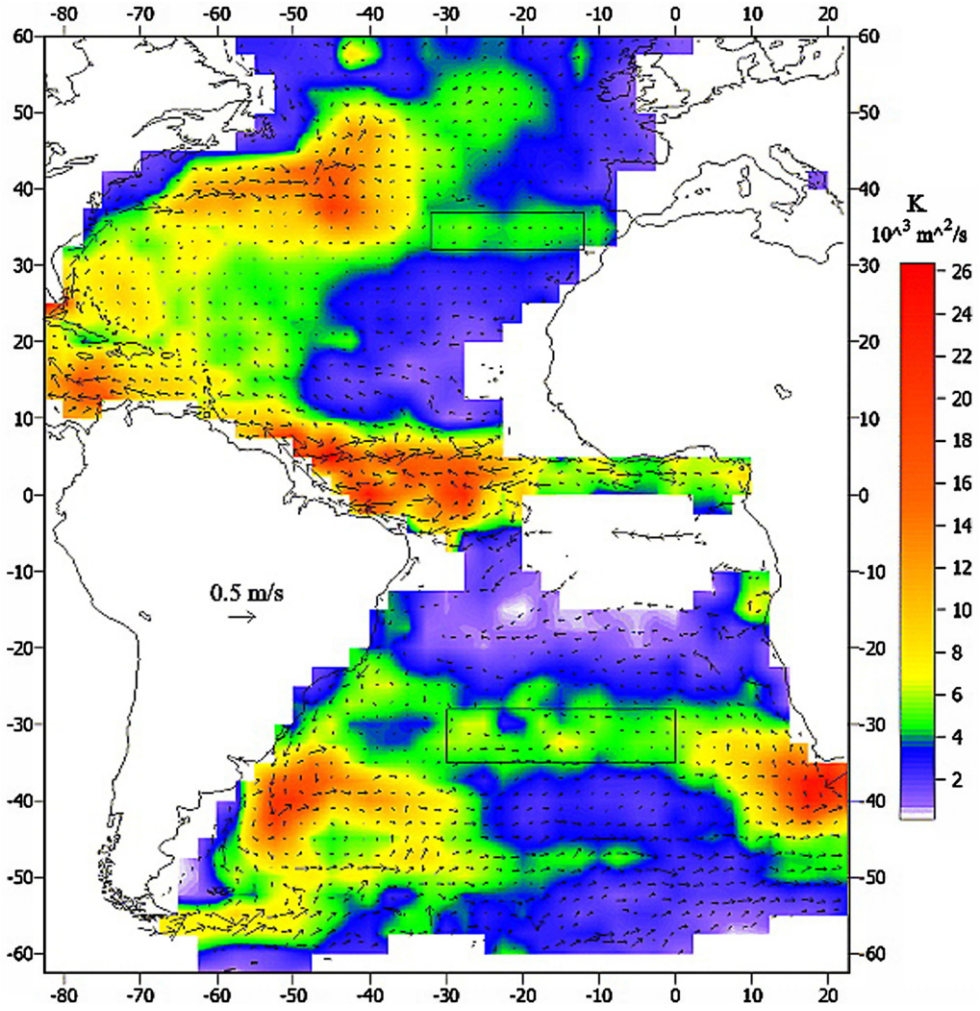


**Fig. 5.** Lateral diffusivities derived from surface drifters in the North Atlantic, from Zhurbas and Oh (2004). Superimposed are the mean velocity vectors, also deduced from the drifters. With permission.

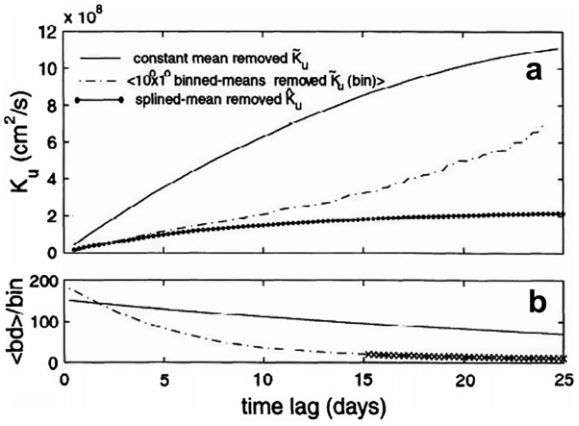


**Fig. 6.** The diffusivity plotted against lag from drifter data in a region of the tropical Pacific. Three different mean fields were used to calculate the residual velocities: a constant one, one obtained from averaging in $10^\circ \times 1^\circ$ rectangles and one derived from spline-fitting. The latter method produces the best convergence. From Bauer et al. (1998), with permission.

aged velocities with splines, the diffusivity converged to a constant value (Bauer et al., 1998). In this case, the spline procedure successfully captured lateral variations in the mean which were below the bin scale.

### 2.3. Stochastic models

As noted earlier, Eq. (18) can be used to predict the spread of tracer in a given area, if the mean velocities and the diffusivities are chosen to match observations. Another approach is to generate synthetic Lagrangian trajectories which share the same dispersion properties as observed, and monitor the spreading of those particles.

This is the idea behind stochastic models. Particle positions are advanced in time, subject to random perturbations. The models are distinguished by where the random forcing is introduced (to the particle position, velocity, acceleration, etc.) and by the number of free parameters involved. In contrast to the tracer equation (18), the stochastic model is a purely Lagrangian construct. Stochastic models have been used in both the atmosphere and ocean to simulate tracer evolution. Discussions are given by Thomson (1987), Zambianchi and Griffa (1994), Griffa et al. (1995), Rodean (1996), Sawford (2001) and Berloff and McWilliams (2002).

The most basic such model is the random walk. In this, the "zeroth-order model", the particle position is the "noised" variable. With a mean background velocity, $\overline{U}$, the model can be written:

$$dx_i = \overline{U}_i dt + \sqrt{2} v_i dw_i, \tag{23}$$

where $v_i$ is the rms velocity in the $i$ direction and $dw_i$ is a Weiner process: a random increment with a Gaussian distribution and unit

variance (Gardner, 2004). Particles disperse in this model and it can be shown that the positional probability evolves according to a Fokker–Plank equation:

$$\frac{\partial}{\partial t}P + \vec{U}\cdot P = \nabla(\vec{\kappa}\nabla P). \tag{24}$$

The probability therefore evolves exactly as the tracer in (18). So we equate the diffusive representation in (18) with a zeroth-order stochastic process.

In relation to most data, the zeroth-order model is overly simplistic. For one, the particle velocities are uncorrelated from step to step, so the velocity autocorrelation is a delta function. This is only sensible if the temporal spacing of the data is larger than the Lagrangian time scale, as for example with ALACE float data. Second, the dispersion always increases linearly in time, so the model misses the quadratic growth expected at early times as in (13). Both aspects stem from the assumption that the turbulent processes occur at length and time scales much smaller than that of the mean flow, $U_i$ (Section 2.2).

Better in these respects is the first-order stochastic model. In this, it is the velocity rather than the displacement which is the noised variable (e.g. Sawford, 1991). The model can be written:

$$\begin{aligned} \mathrm{d}x_i &= (u_i + \overline{U}_i)\mathrm{d}t, \\ \mathrm{d}u_i &= -\frac{1}{T_i}u_i\mathrm{d}t + \sqrt{\frac{2}{T_i}}v_i\mathrm{d}w_i. \end{aligned} \tag{25}$$

The velocities thus have two contributions, the random perturbation plus a term which represents the memory of the previous velocity and is inversely proportional to the integral time, $L_i$. This term causes the velocity autocorrelations to decay exponentially:

$$R_i = \mathrm{e}^{-t/T_i}. \tag{26}$$

The model also correctly captures the early and late behavior in (13) and (14).

The Fokker–Plank equation associated with the first-order model is somewhat more complicated than with the zeroth-order model (Zambianchi and Griffa, 1994):

$$\frac{\partial}{\partial t}P + (\vec{U}+\vec{u})\cdot P + \nabla_u(\vec{u}P/T) = \nabla_u(\vec{\kappa}\nabla_u P). \tag{27}$$

The gradients in the last two terms are evaluated with respect to the velocities rather than to the spatial variables. Tracer evolves somewhat differently under (27) than under (18), particularly at times comparable to the integral scale (Zambianchi and Griffa, 1994).

The first-order model has been used to simulate the dispersion of surface drifters (Griffa et al., 1995; Falco et al., 2000) and subsurface floats (Veneziani et al., 2004). It has also been used to mimic the dispersion of synthetic floats in numerical ocean models (Berloff and McWilliams, 2002) and of pollutants in the atmospheric boundary layer (Wilson and Sawford, 1996).

While the velocities are uncorrelated in time in the zeroth-order model, the accelerations are uncorrelated in the first-order model. This is appropriate if the temporal resolution of the data is insufficient to capture changes in the drifter velocity. But if the accelerations are resolved, one could use a second-order stochastic model, in which the acceleration is the noised variable (Sawford, 1991). This can be written:

$$\begin{aligned} \mathrm{d}x_i &= (u_i + \overline{U}_i)\mathrm{d}t, \\ \mathrm{d}u_i &= a_i\mathrm{d}t - \frac{1}{T_{vi}}u_i\mathrm{d}t, \\ \mathrm{d}a_i &= -\frac{1}{T_{ai}}a_i\mathrm{d}t + \left(\frac{2(T_{ai}+T_{vi})}{T_{ai}T_{vi}}\right)v_i\mathrm{d}w_i, \end{aligned} \tag{28}$$

where $T_{vi}$ and $T_{ai}$ are the decay time scales associated with the velocity and acceleration respectively. The resulting autocorrelation is a difference between two exponentials (Sawford, 1991; Rupolo, 2007), and is thus more complex than that in the first-order model. Berloff and McWilliams (2002) also used the second-order model to simulate trajectories in their idealized ocean model.

Whether the acceleration time scale is resolved in the data was examined by Rupolo et al. (1996) and Rupolo (2007). In the latter work, the author fit observed velocity autocorrelations to determine the time scales $T_v$ and $T_a$. Shown in Fig. 7 is the ratio $T_a/T_v$ from drifters and floats in the North Atlantic. At the surface, the ratio is small in the eastern and central basin, implying the acceler-

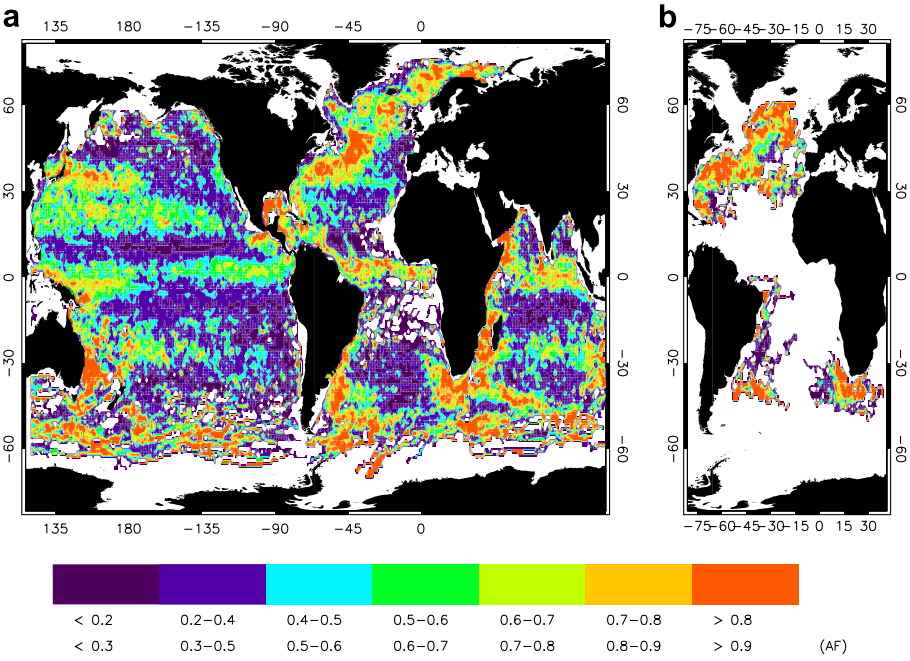


**Fig. 7.** The ratio of the acceleration time scale, $T_a$, to the velocity time scale, $T_v$. The left panel derives from surface drifter data, and the right from subsurface float data. From Rupolo (2007), with permission.

ation time scale is not well resolved. The ratio approaches one however in the west.

The floats provide a similar picture, except that the ratio is larger over more of the basin (the eastern basin is not resolved due to a lack of data). This suggests the accelerations are better resolved in the float data in than in the drifter data, most likely because the integral time is larger at depth (Sections 2.7 and 2.8).

The difference between large and small ratio trajectories is clearly seen. While drifters with large ratios of $T_a/T_v$ have smooth trajectories, drifters with small ratios have a more jagged appearance, because the drifters are changing direction on time scales shorter than the resolution of the data. Thus higher-order models are more appropriate when simulating dispersion in the energetic western regions, and at depth.

An interesting aspect of the second order model is that it can yield either real or complex values for $T_v$ and $T_a$. With complex values, the autocorrelation exhibits oscillatory behavior in addition to decay. In this case, the second order model is equivalent to a two-dimensional first order model, with the two horizontal velocity components coupled (Reynolds, 2002). In this model, particles *loop*, much as drifters and floats often do in the ocean (e.g. Richardson, 1993). Because the looping alters the autocorrelation, it also affects the dispersion (Pasquero et al., 2001). A number of authors have

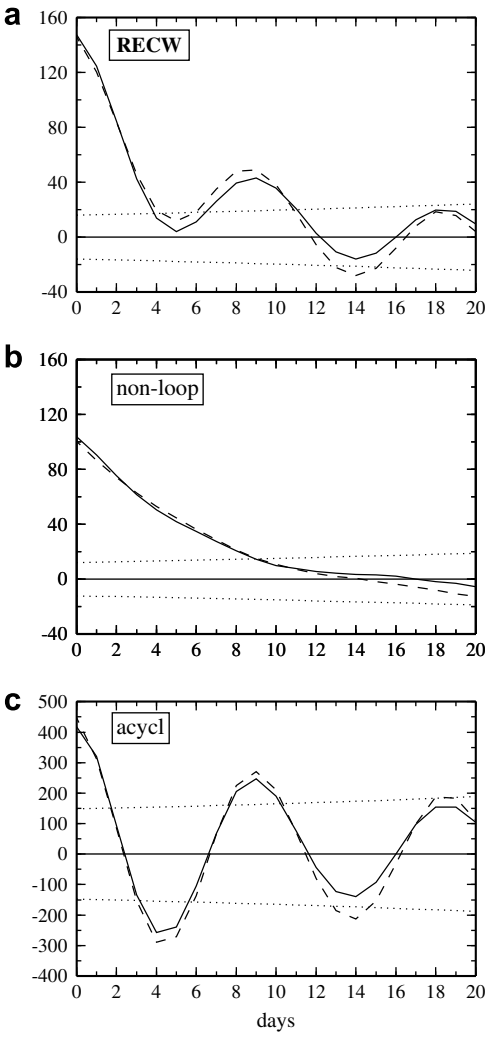


**Fig. 8a.** Velocity autocorrelations from a set of subsurface floats in the western North Atlantic. The results from the full set, the non-looping and looping subsets are shown in the upper/middle/lower panels. The solid/dashed curves correspond to the zonal/meridional correlations.

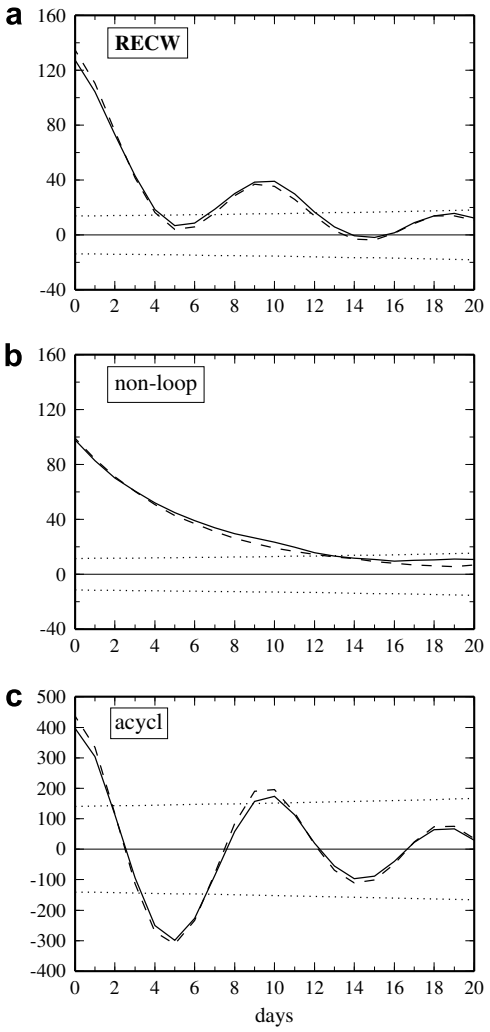


**Fig. 8b.** The corresponding autocorrelations from a first-order stochastic model with rotation. From Veneziani et al. (2004), with permission.

examined the properties of such a model (Borgas et al., 1997; Sawford, 1999; Berloff and McWilliams, 2002; Veneziani et al., 2005; Reynolds, 2003; Veneziani et al., 2004). The first order model with rotation can be written:

$$\begin{aligned} du &= -\frac{1}{T_x}u dt + \Omega v dt + \left(\frac{2}{T_x}\right)^{1/2} v_x dw_x, \\ dv &= -\frac{1}{T_y}v dt - \Omega u dt + \left(\frac{2}{T_y}\right)^{1/2} v_y dw_y. \end{aligned} \tag{29}$$

The rotational terms resemble the vertical Coriolis terms in the horizontal momentum equations and couple the $u$ and $v$ velocities. The resulting autocorrelations oscillate with lag:

$$R_x = e^{-t/T_x}\cos(\Omega t), \quad R_y = e^{-t/T_y}\cos(\Omega t). \tag{30}$$

The autocorrelations thus do not decay monotonically but exhibit a negative lobe. As a result, the diffusivity, proportional to the integral of the autocorrelation, first increases with lag then decreases, before leveling off.

Veneziani et al. (2004) used such a model to simulate float dispersion in the North Atlantic. In the data sets they examined, roughly one third of the floats looped, with different rotational rates. So they treated the rotationally frequency, $\Omega$, as a random variable with approximately the same distribution as observed. The distribution is generally trimodal, reflecting non-loopers (zero

spin) and loopers with positive and negative spin (cyclones and anticyclones).

An example, for floats in the western part of the recirculation south of the Gulf Stream, is shown in Fig. 8. There is an eastward mean flow here, but the rms residual velocity is greater by roughly a factor of 6. The non-looping floats (middle left panel) exhibit a monotonically decaying autocorrelation, similar to the exponentially decaying correlation from the stochastic routine (middle right panel). In contrast, the autocorrelations from the looping trajectories (lower panels) exhibit pronounced oscillations. The autocorrelations from the combined set (upper panels) are thus decaying and oscillating. The agreement between the stochastic model and the data is striking, and similar results were obtained in the other regions they examined.

The authors also calculated the cross-correlations between the horizontal velocities. The non-loopers had zero correlation between $u$ and $v$, within the errors, while the loopers had significant, and oscillating, correlations. Thus, the looping floats alone account for the off-diagonal terms in the diffusivity matrix (Section 2.2.2).

Calculations like those of Veneziani et al. (2004) are usually made in restricted regions so that the eddy variability is approximately homogeneous. Constructing models which account for inhomogeneity is more difficult, and care is required to avoid effects such as the spurious generation of tracer gradients (Thomson, 1987). Stochastic models are also generally non-unique, so that there is no single representation for a given data set. These models nevertheless are very promising for predicting tracer evolution.

### 2.4. PDFs

As noted, the displacement moments derive from the displacement PDF, $Q(X,t)$. Closely related is the PDF of residual velocities, $Q(u\prime,t)$. The advective–diffusive formalism of Davis (1991) and the stochastic models assume that $Q(X,t)$ and $Q(u\prime,t)$ are approximately Gaussian. Swenson and Niiler (1996) checked this, in their analysis of drifter data from the California Current, and concluded the velocity PDFs were not significantly different from Gaussian.

Bracco et al. (2000a) made a similar calculation, using data from subsurface floats in the North Atlantic. They did this by combining residual velocities from a large region, such as the western Atlantic, after first correcting for regional variations in eddy energy (by binning the velocities, de-meaning them and then dividing by the local standard deviation of the residual velocity). This approach greatly increased the degrees of freedom, and hence the accuracy of the PDFs.

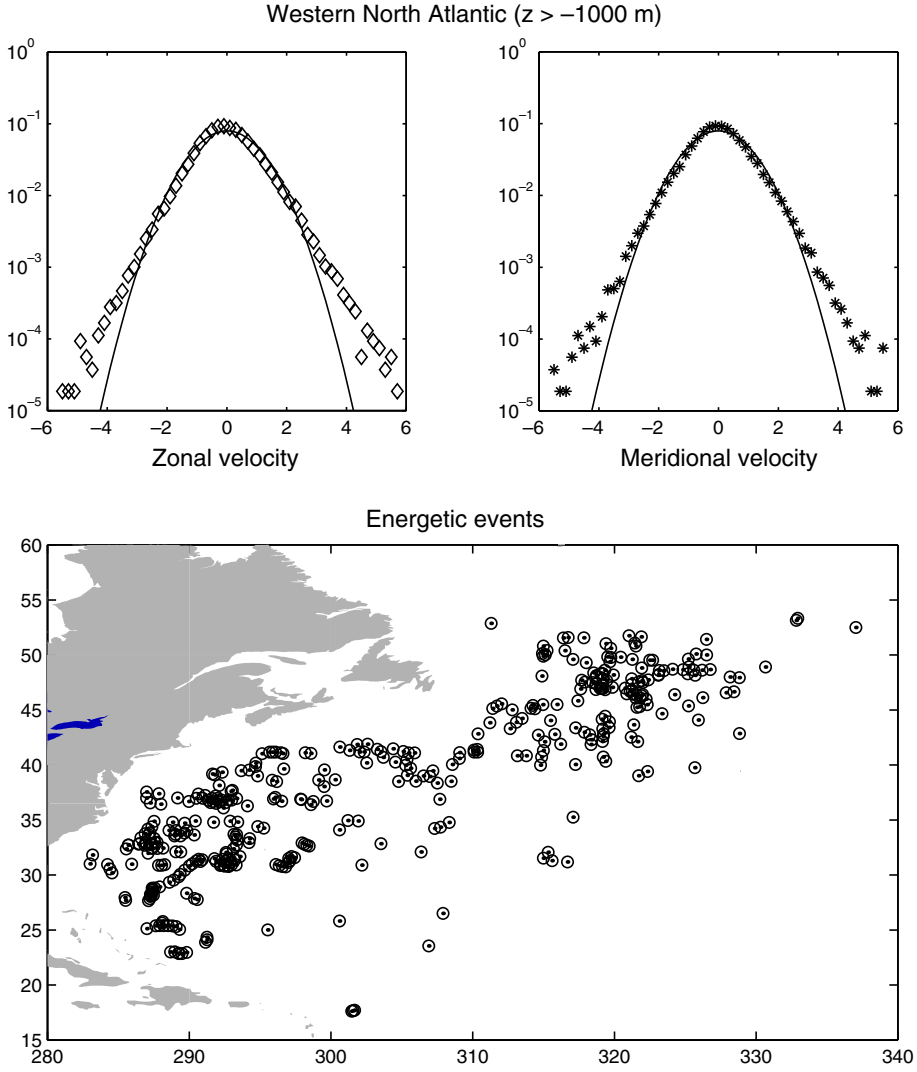


**Fig. 9.** Velocity PDFs from subsurface float data from the upper 1000 m of the western North Atlantic. The upper panels show the zonal and meridional velocity distributions, and the lower panel shows the locations of energetic events (residual velocities greater than two standard deviations). The latter are spread over the region covered by the floats and indicate multi-day advection events. From Bracco et al. (2000a).

An example, from the shallow Northwest Atlantic, is shown Fig. 9. Both the zonal and meridional velocity PDFs deviate significantly from a Gaussian in that the tails of the distribution are extended. The latter are actually nearer to an exponential distribution than a Gaussian. The deviations are significant as measured by the Kolmogorov–Smirnov (K–S) test (D'Agostino and Stephens, 1986).

The extended tails reflect an excess of velocities several times the standard deviation. These extreme events occur over the whole region (lower panel) and are often associated with coherent advection, e.g. rapid translation or looping, which lasts a few days. In this region, the events are most likely associated with the Gulf Stream. However, Bracco et al. (2000a) found similar PDFs in the deep western Atlantic, below the core of the stream, and also in the more quiescent eastern Atlantic. Similarly non-Gaussian PDFs were subsequently found in the Adriatic Sea (Maurizi et al., 2004) and the Mediterranean (Isern-Fontanet et al., 2006). Only near the equator are the PDFs nearly Gaussian (Bracco et al., 2000a).

Nearly the same type of non-Gaussian PDF are found in numerical simulations of 2-D turbulence, where the large velocity events are linked to advection by coherent vortices (Jimenez, 1996; Weiss et al., 1998; Bracco et al., 2000a,b). If this is the same situation in the ocean, we would infer there are fewer such vortices at low latitudes.

In principle, the PDF derived from Lagrangian velocities should be the same as that derived from Eulerian velocities, assuming the coverage of both data sets is sufficiently uniform (Tennekes and Lumley, 1972; Bennett, 2006). This was confirmed by the author, who compared the float- and current meter-derived PDFs from the western North Atlantic. The current meter PDFs are similarly non-Gaussian and statistically identical (by the Kolmogorov–Smirnov test) to the float PDFs from the same region (Fig. 10).

Because extreme events are rare, one requires long time series (or a large set of shorter time series) to capture them. The deviations from Gaussianity moreover are relatively modest. The kurtosis (Section 1.2) is typically about 4.0, only somewhat larger than the Gaussian value of 3.0. As noted earlier, the advective–diffusive formalism of Section 2.2 assumes the Lagrangian velocities are normally distributed, and the differences seen here are probably small enough so as not to warrant concern.

### 2.5. Alternate stationary coordinates and $f/H$

We have until now considered velocities and displacements in Cartesian coordinates, i.e. in the zonal and meridional directions. This is reasonable so long as any anisotropy in the dispersion is either in the east–west or north–south direction. Atmospheric dispersion is typically zonally anisotropic, due primarily to the $\beta$-effect. In the ocean on the other hand, the dispersion can be influenced by bottom topography, whose orientation varies with location.

The topographic influence is greatest for a barotropic fluid. Consider the linear shallow water vorticity equation:

$$\frac{\partial}{\partial t}\nabla\times\bar{\mathbf{u}}+J\left(\psi,\frac{f}{H}\right)=\nabla\times\left(\frac{\tau_w}{\rho H}\right)-\nabla\times\left(\frac{\tau_B}{\rho H}\right), \tag{31}$$

where $\bar{\mathbf{u}}$ is the depth-averaged velocity, $\psi$ the transport streamfunction, $H(x,y)$ the water depth and $\tau_w$ and $\tau_B$ are the surface wind and bottom stresses. Without forcing and dissipation, the vorticity changes only when there is motion across the $f/H$ contours. As such, $f/H$ provides a restoring force, supporting Rossby and/or topographic waves.

Were the ocean barotropic and unforced, we would expect greater dispersion along $f/H$ than across (LaCasce and Speer, 1999). One way to test for this is to project float displacements onto and across the $f/H$ contours and calculate the dispersion from the projected displacements (LaCasce, 2000). An example, using floats from the North Atlantic Current (NAC) experiment in the shallow northwest Atlantic (Zhang et al., 2001), is shown in Fig. 11.[8] The trajectories are shown in the upper panel, superimposed on $f/H$. Shown in the lower panels are the mean displacements and the dispersions plotted against time. In zonal/meridional coordinates, the dispersion is isotropic within the errors and the mean displacements indicate a drift to the northwest. But the dispersion is significantly anisotropic with respect to $f/H$, with greater spreading along the contours. The mean drift is also aligned with $f/H$, and the drift across $f/H$ is not significantly different from zero.

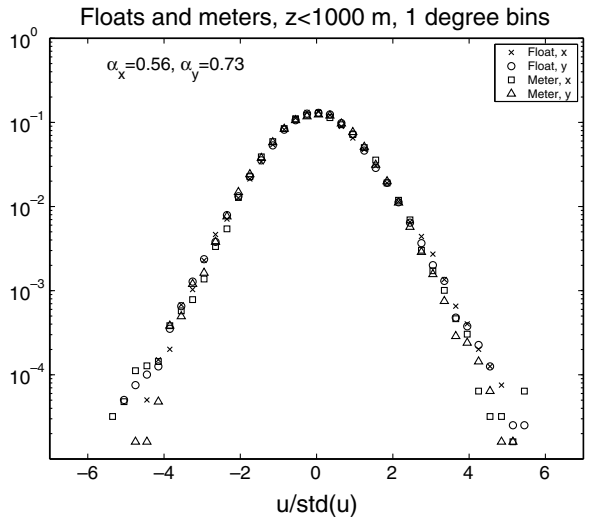


**Fig. 10.** The velocity PDFs derived from float data, normalized using 1° degree bins, and from current meter data. Both sets of data come from the upper 1000 m of the western North Atlantic. The numbers at upper left are the probabilities that the distributions are the same, from the Kolmogorov–Smirnov test; these indicate the null hypothesis (that they are different) cannot be rejected. From LaCasce (2005).

Evidently the floats are steered by $f/H$, a fact not apparent from the statistics in $x$—$y$ coordinates. This is remarkable, given that the floats are only 100–200 m deep! Indeed, the floats are clearly constrained in their lateral spreading by the mid-Atlantic ridge, despite that the latter lies over 1000 m beneath them.

To test the hypothesis of topographic steering, we can make the same calculations with stochastically generated float trajectories. To do this, we use the first-order model in (25) with the mean velocities, $U$ and $V$, the integral time scales, $T_x$ and $T_y$, and the variances calculated from the float data. The results are shown in Fig. 12.

The stochastic trajectories resemble those of the actual floats, covering roughly the same region. But the stochastic float dispersion is isotropic, both with respect to $(x,y)$ coordinates and to $f/H$, and the mean drift moreover is across $f/H$. We conclude that the stochastic floats do not feel the topography.

O'Dwyer et al. (2000) made a similar calculation to compare float displacements with in situ potential vorticity derived from hydrography. They also found evidence for steering. This in turn suggests the baroclinic PV in the North Atlantic is correlated with barotropic $f/H$.

Some have exploited topographic steering when calculating bin-averaged mean velocities (Section 2.2.1). Davis (1998) calculated his averages using a weighting function which accounted for the longer spatial correlations expected along $f/H$ contours. Fischer and Schott (2002) and Lavender et al. (2005) used a similar

[8] These are subsurface floats designed to follow isopycnals. As such, the float depths vary, but are generally less than 800 m.

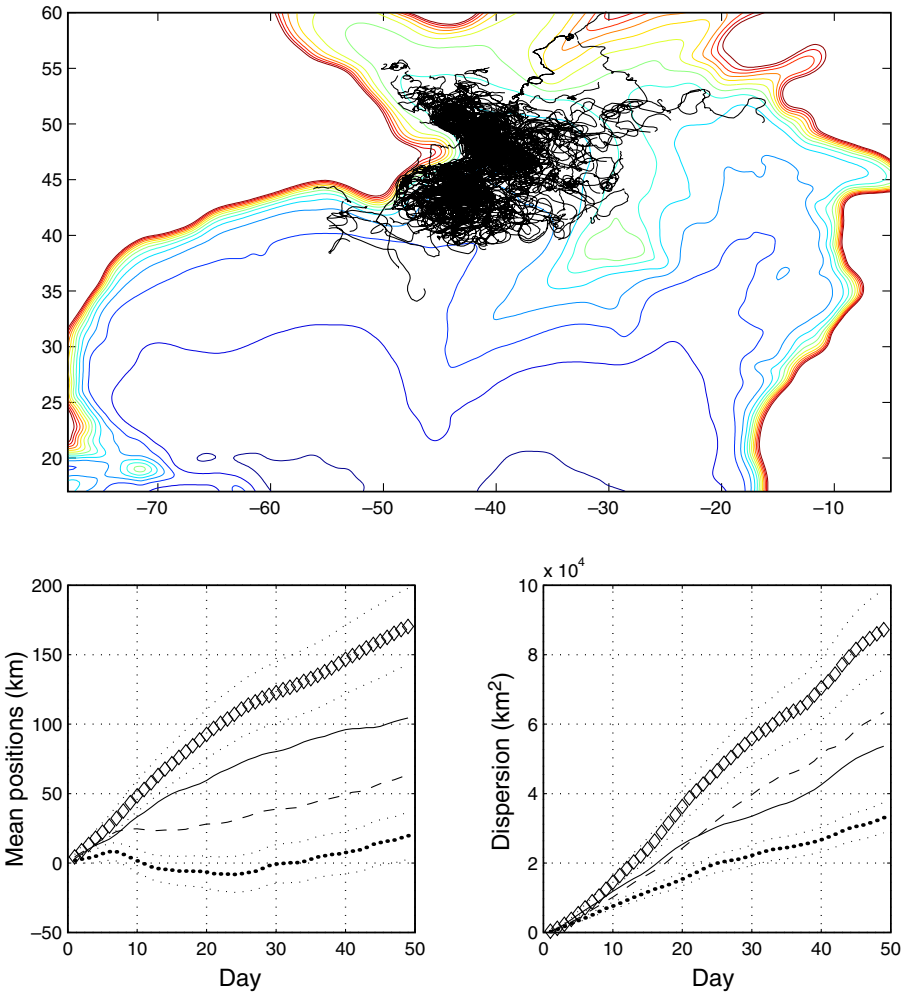


**Fig. 11.** The trajectories of floats from the western North Atlantic, superimposed on contours of f/H. The lower panels show the mean displacements and dispersion relative to latitude (solid) and longitude (dashed), and along (diamonds) and across (dots) $f/H$. The dotted lines for the $f/H$ curves indicate the 95% confidence limits. From LaCasce (2000).

approach when calculating subsurface mean velocities in the Labrador Sea and the subpolar North Atlantic.

*2.5.1. Rossby waves*

One way for floats to drift along $f/H$ contours is to be advected by Rossby waves. This was shown in two important studies. Freeland et al. (1975) used objective mapping to convert SOFAR float velocities into a time-evolving streamfunction, which they then used to construct Hovmöller diagrams. These showed clear evidence of westward phase propagation. Price and Rossby (1982) studied a set of SOFAR floats, from the local dynamics experiment (LDE) in the western North Atlantic, which were clearly oscillating back and forth across $f/H$ contours. By computing velocity correlations lagged in both space and time, they deduced phase propagation to the Northwest, or westward relative to $f/H$. This was evidently a mixed planetary/topographic wave.

Like gravity waves, Rossby waves can have a Stokes-type drift, as demonstrated by Flierl (1981) for a wave in a zonal channel. The magnitude of the drift depends on the ratio of the rms particle speed to the phase speed. For small values of the ratio, the particles oscillate about $f/H$, precessing slowly along the contours. The drift is either parallel or antiparallel to the phase speed (i.e. west or east relative to $f/H$). If instead the ratio is of order one, the wave *traps* a volume of fluid and sweeps it westward, at the wave phase speed. In this case, the wave vorticity is strong enough so that there are closed streamlines in the frame moving with the wave. In both of the observed cases above, the inferred wave phase speed and the rms float velocities were comparable (of order of 5 cm/s), so the floats were quite possibly being swept along in this manner.

It remains to be seen whether this is a common occurrence or not. Free Rossby waves, for instance radiating from a localized source (e.g. Spall et al., 1993), do not induce drift in the same way as channel waves. Nevertheless, it is possible that finite amplitude Rossby waves represent an effective transport mechanism in the ocean.

*2.6. Non-stationary fields: correlations with scalars*

One can also calculate correlations between float displacements and non-stationary fields. Consider the Reynolds-averaged temperature equation:

$$\frac{\partial}{\partial t}T + \nabla\cdot(\overline{\mathbf{U}}\overline{T}) + \nabla\cdot(\overline{\mathbf{u}'T'}) = S + M, \tag{32}$$

with the terms on the right hand side representing sources (e.g. surface heating) and small-scale mixing. The eddy transport term on the left side can in principle be evaluated directly using Lagrangian data.

Swenson and Niiler (1996) made such a calculation, using data from temperature-recording surface drifters in the California current. They calculated residual velocities and temperatures by sub-

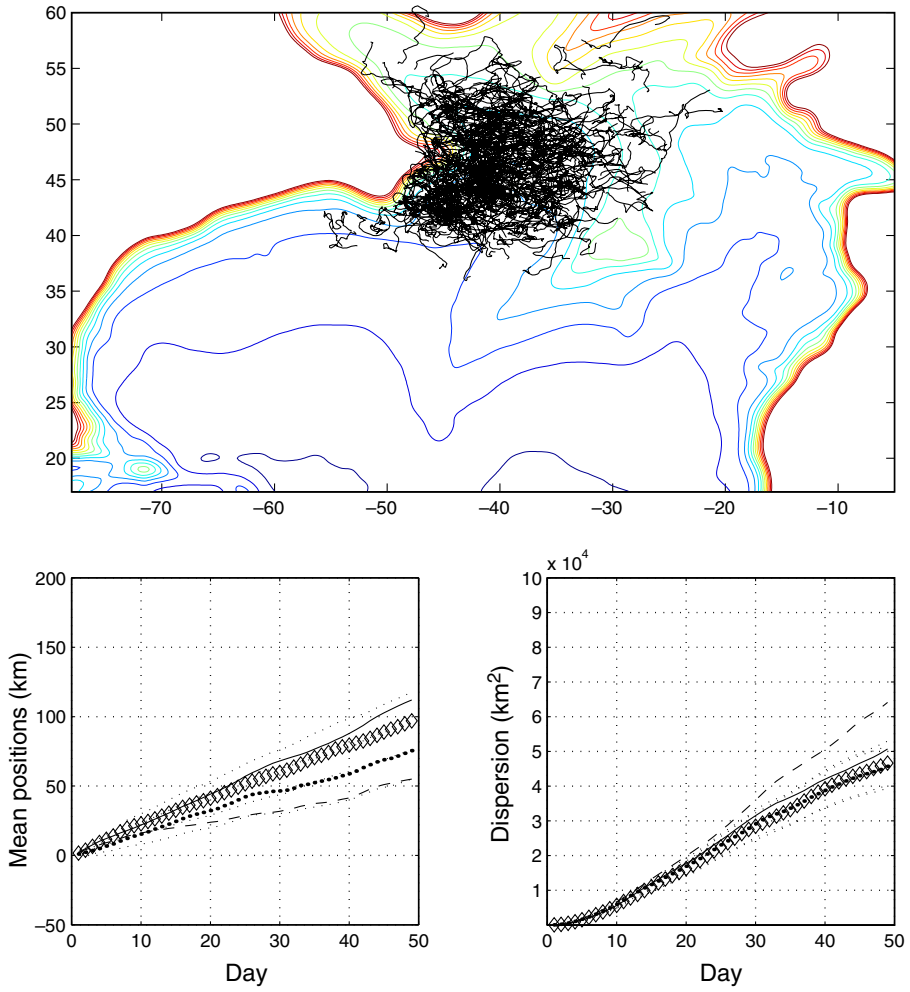


**Fig. 12.** Float trajectories generated using a first-order stochastic model, with identical mean and variances as the floats shown in Fig. 11. From LaCasce (2000).

tracting the time–mean velocity and temperature for each drifter, and then averaged the products. The resulting eddy flux divergence was roughly an order of magnitude smaller than the mean advection of heat (inferred from the binned drifter velocities and the mean temperature gradient from satellite-derived SST). Swenson and Niiler also compared the direct eddy flux estimates with those obtained from a diffusive parameterization, i.e.:

$$\nabla \cdot (\overline{\mathbf{u}'T'}) = -\nabla(\kappa \nabla \overline{T}).$$

To evaluate the RHS, they used the drifter-derived diffusivities with the satellite-derived mean temperature gradient. The two estimates agreed within the errors, a remarkable result which supported both the eddy divergence calculation and the diffusive parameterization.

Gille (2003) similarly calculated eddy heat fluxes using data from ALACE floats at 900 m depth in the Southern Ocean. As noted before, the ALACE float is not tracked continuously, but Gille was able to obtain flux estimates nevertheless. Her estimates were consistent with previous calculations using current meter data and hydrography. However she found poor agreement with the flux calculated from the mean temperature gradient, at odds with a simple diffusive parameterization. So the applicability of the parameterization may vary with location.

### 2.7. Frequency spectra

As noted in Section 2.1, the Lagrangian frequency spectrum is related to the velocity autocorrelation by the Fourier transform. Thus the spectrum can advantageously reveal temporal aspects of the dispersion. Spectra have been calculated from float data (Freeland et al., 1975; Rupolo et al., 1996; Rupolo, 2007) and from drifter data (Colin de Verdiere, 1983; Krauss and Böning, 1987; Lumpkin and Flament, 2001; Rupolo, 2007).

What type of spectra should one expect? Consider an exponentially decaying autocorrelation, as obtained with a first-order stochastic model (Section 2.3). This yields

$$T(\omega) = 2\int_0^\infty \exp(-t/T_L)\cos(2\pi\omega t)\mathrm{d}t = \frac{2T_L^{-1}}{T_L^{-2} + 4\pi^2\omega^2}. \qquad (33)$$

This exhibits an $\omega^{-2}$ decay at high frequencies and a white spectrum at low frequencies, with a transition frequency of $\omega = (2\pi T_L)^{-1}$. The spectrum at low frequencies is white because the integral of the autocorrelation converges (were it red, no diffusivity would exist; e.g. Colin de Verdiere, 1983).

The spectra for various ocean basins are shown in Fig. 13, from Rupolo (2007). These derive from drifters in the North Atlantic, Arctic, Pacific and Indian oceans, and from floats in the North Atlantic. Both the zonal and meridional spectra are plotted.

The low frequency drifter spectra are in most cases anisotropic. While the meridional spectra are nearly white at time scales greater than about 10 days, the zonal spectra are red. The exceptions are the floats in the North Atlantic and the drifters in the Arctic, for which the spectra are nearly isotropic.

The anisotropy may reflect the influence of $f/H$ (Section 2.5). In the Pacific, the $f/H$ contours are mostly zonal, favoring zonal

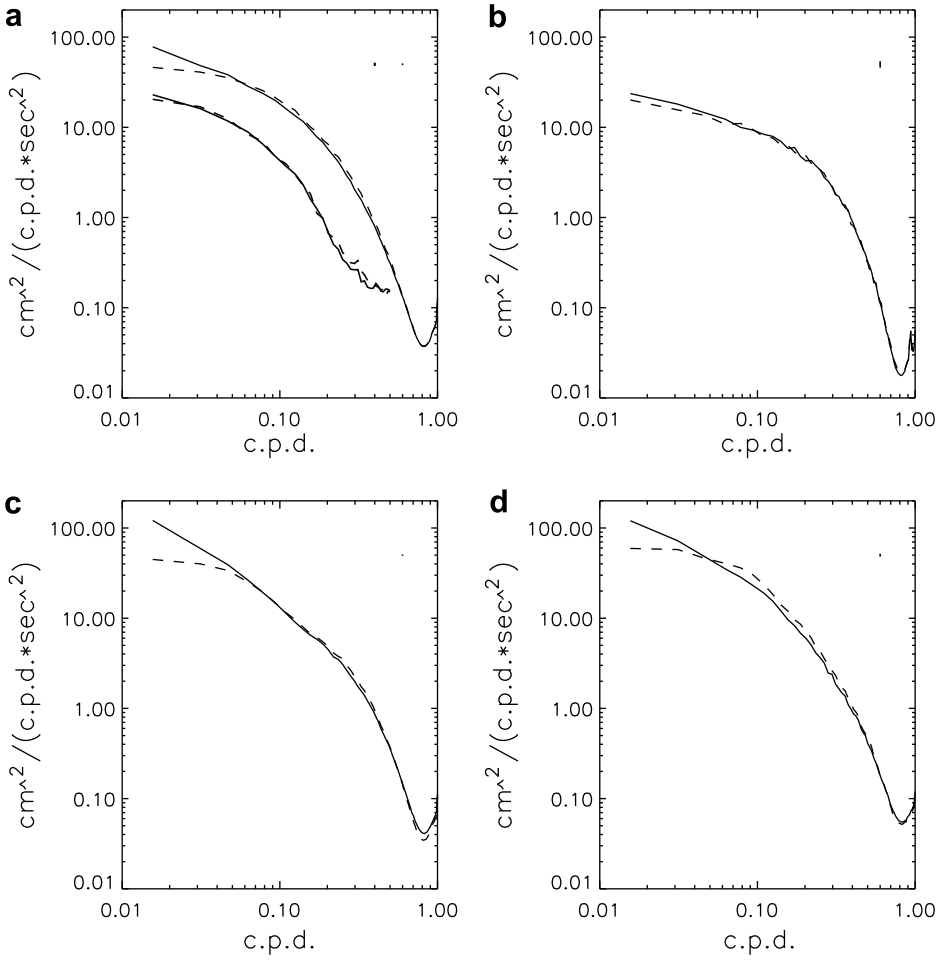


**Fig. 13.** Lagrangian frequency spectra. The upper left panel shows zonal (solid) and meridional (dashed) spectra from drifters (thin lines) and floats (thick lines) in the North Atlantic. The other panels show spectra from drifters in the Arctic region (upper right panel), the Pacific (lower left) and the Indian Ocean (lower right). From Rupolo (2007), with permission.

spreading. Similarly zonally anisotropic dispersion was seen by Hogg and Owens (1999) in the Argentine basin, where the $f/H$ contours are also mostly zonal. The $f/H$ contours in the Atlantic and Arctic basins on the other hand are greatly distorted by topography, and this can produce apparently isotropic spreading (Fig. 11). It is possible the spectra would be anisotropic if calculated with velocities projected along and across $f/H$.

It is interesting that the drifters in the North Atlantic exhibit low frequency anisotropy while the floats don't. This may reflect the different spatial distributions of the data. While the drifters span the basin, the floats are concentrated in the western basin at mid-latitudes (e.g. Fig. 7), where topography severely contorts the $f/H$ contours.

In the North Atlantic, the energy levels are much greater at the surface than at depth. The integrated kinetic energy for the Atlantic drifters is 331 $cm^2/s^2$ while that for the floats is only 89 $cm^2/s^2$ (Rupolo, 2007). This difference implies a similar difference in the diffusivities (Section 2.1). Lumpkin et al. (2002) likewise found that the surface diffusivities in the North Atlantic were an order of magnitude larger than those at 1500 m depth.

When it comes to the higher frequencies, all the spectra are isotropic and the slopes are approximately the same. This also applies to the North Atlantic floats, suggesting the high frequency motion at the surface is mirrored at depth. As noted above, the transition frequency between the low and high frequency ranges is proportional to the inverse Lagrangian time scale. We see in Fig. 13 that this transition occurs at a lower frequency for the Atlantic floats than for the drifters. Accordingly, the Lagrangian time scale for the drifters is roughly 2–3 days, in all four basins, and roughly twice that for the floats (Lumpkin et al., 2002; Rupolo, 2007).

### 2.8. Euler–Lagrange transformations

Lastly, we consider the connection between Lagrangian and Eulerian statistics. If the Lagrangian integral time is 5 days, can we predict the Eulerian integral time? Quantifying this connection is important for using Lagrangian measurements in (Eulerian) model parameterizations.

Corrsin (1959) proposed such a connection, as follows. In the Eulerian frame, velocity correlations decay in both space and time. So the velocities at a single location will become decorrelated after a period of time (the Eulerian integral time), and two observers separated by more than a certain distance (the Eulerian integral scale) will see uncorrelated velocities. A Lagrangian observer, by drifting, experiences both the temporal and spatial decorrelations simultaneously. So the integral time measured by the Lagrangian observer will generally be shorter than that measured by a fixed observer.

Corrsin's conjecture is that the Lagrangian autocorrelation can be derived from the Eulerian spatial-temporal autocorrelation if one knows the PDF of particle displacements, $Q$:

$$R_L(t) = R_{E11}(X,t)Q(X,t)dX. \tag{34}$$

Here $R_{E11}$ is the longitudinal Eulerian correlation (that related to the velocities parallel to the line connecting the two observation points). The relation makes sense because the integral over the displacement PDF reflects how far an average particle wanders from its starting position and thus how much the spatial decorrelation affects the Lagrangian autocorrelation.

Davis (1982, 1983) examined Corrsin's conjecture in the oceanic context. Middleton (1985) applied the conjecture by assuming certain forms for the Eulerian energy spectrum. Both authors obtained analytical results by assuming the displacement PDF was stationary and Gaussian. Middleton's result depends on the ratio of the Eulerian integral time to the advective time, $T_a \equiv L_E/v$ (where $L_E$ is the Eulerian length scale and $v$ the rms velocity) and is appealingly simple:

$$T_L/T_E \approx \frac{q}{(q^2+\alpha^2)^{1/2}}, \tag{35}$$

where $\alpha \equiv T_E/T_a$ and $q \equiv (\pi/8)^{1/2}$. If we write $L_L = vT_L$, then we also have

$$L_L/L_E \approx \frac{\alpha q}{(q^2+\alpha^2)^{1/2}}. \tag{36}$$

Thus if $\alpha \ll 1$, the time scales are approximately equal. If instead $\alpha \gg 1$, then $L_L \approx qL_E$ and the Lagrangian time scale is small compared to the Eulerian. Interestingly, relations (35) and (36) are relatively insensitive to the shape of the Eulerian spectrum (Middleton, 1985).

We can rationalize these results as follows. If a tracer, $S$, is conserved on a Lagrangian parcel, then

$$\frac{dS}{dt} = \frac{\partial}{\partial t}S + \vec{u}\cdot\nabla S = 0. \tag{37}$$

The ratio of the advective term to the tendency term scales as

$$\frac{vT_E}{L} = \frac{T_E}{T_a} = \alpha. \tag{38}$$

Thus if $\alpha \ll 1$, the tendency term dominates, implying the Eulerian velocities decorrelate faster in time than in space. This is referred to as the "fixed float" regime. If instead $\alpha \gg 1$, the advective term dominates. So the drifters move rapidly from their starting positions and the spatial variations of the Eulerian velocities determine the Lagrangian decorrelation. This is the "frozen turbulence" regime.

Lumpkin et al. (2002) checked relations (35) and (36) using data from the 1/3° MERCATOR model of the North Atlantic. The relations worked remarkably well, over a range of values of $\alpha$ (their $u'/c_*$; Fig. 14), both at the surface and at depth. An assessment of the relation using in situ data has not yet been made (and would be difficult, given the need for extensive and simultaneous Lagrangian and Eulerian data), but Lumpkin et al.'s results are promising. Thus Middleton's relations could be used as a basis for converting Lagrangian diffusivities to Eulerian ones.

Note in Fig. 14 that the Lagrangian time scales are shorter at the surface than at depth. The same result was inferred from the Lagrangian spectra (Section 2.7). In addition, the Lagrangian length scales are consistently larger at the surface than at depth.

### 2.8.1. Diffusivity scaling

A drawback with the advective–diffusive formalism of Section 2.2 is that direct observations are required to determine the diffusivity. It would be advantageous if one could instead infer the diffusivity independently, for example from satellite measurements.

Some studies indicate the diffusivity scales with eddy kinetic energy (Price, in McWilliams et al., 1983; Poulain and Niiler, 1989; Figueroa and Olson, 1989):

$$\kappa \propto v^2 T,$$

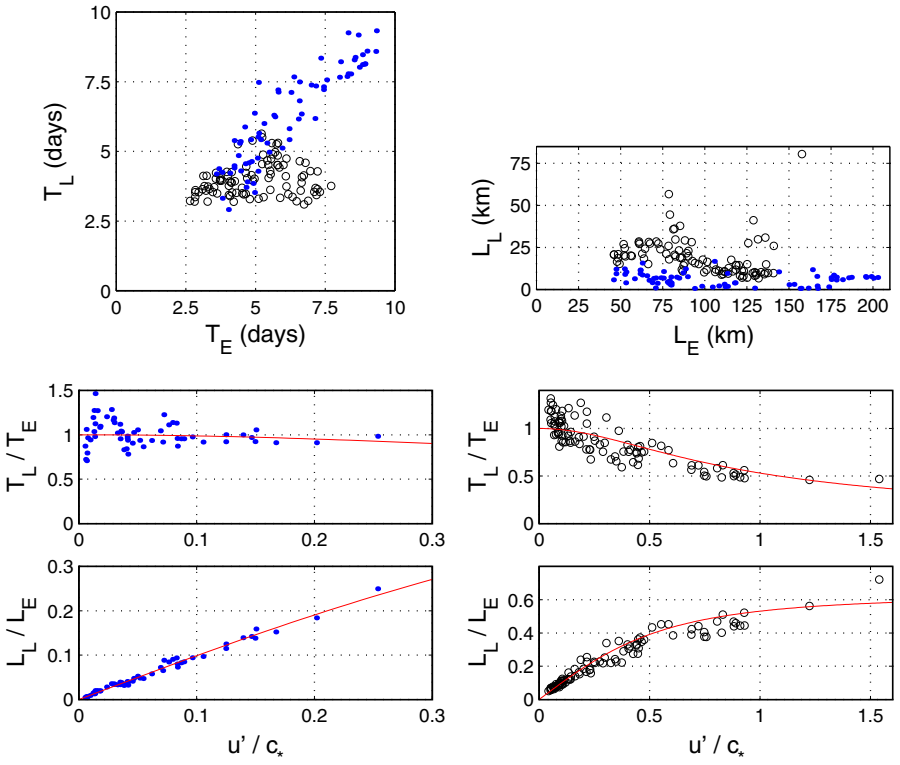


**Fig. 14.** The ratio of Eulerian and Lagrangian time and length scales from floats seeded in a numerical model of the North Atlantic (lower panels). The red curves are the predictions from Middleton (1985). The upper panels are scatter plots for the time and length scales for particles at the surface (open circles) and in the deep layers (blue points). From Lumpkin et al. (2002), with permission.

where $T$ is a constant time scale. This would be appropriate if the integral time were everywhere constant. Others have suggested the diffusivity scales with the rms velocity (e.g. Krauss and Böning, 1987; Brink et al., 1991; Zhang et al., 2001):

$$\kappa \propto vL,$$

which would make sense if the integral length scale, $L$, was constant. Of course if the time scale, $T$, is the advective time scale, i.e. $T_a \propto L_E/v$, the estimates are the same. Swenson and Niiler (1996) suggested such a situation applies in the California current.

From the discussion in Section 2.8, we identify the first case, with a constant time scale, with the fixed-float regime and the second, with a constant length scale, with the frozen turbulence regime. Lumpkin et al.'s (2002) results suggest that neither regime applies over the whole North Atlantic. Rather, the frozen regime applies in regions with energetic eddies, such as near the unstable boundary currents, while the fixed-float regime applies in relatively quiescent regions, such as the eastern North Atlantic (as also suggested by Rupolo, 2007).

## 3. Multiple particles

Relative dispersion, the mean square distance between pairs of particles, concerns how a cloud of tracer spreads about its center of mass (Section 1.2). It also measures the sensitivity of Lagrangian trajectories to their initial position. Lagrangian chaos is an example in which particles deployed near one another diverge exponentially in time. As seen below, relative dispersion has the same early and late time asymptotic behavior as absolute dispersion. However, its behavior at intermediate times often depends revealingly on the Eulerian flow (Section 3.1). For this reason, relative dispersion has long been of interest in turbulence studies.

Richardson (1926) initiated the study with his work on the dispersion of smoke plumes from factories and of balloons. He observed that the dispersal rate increased with cloud size, implying the *relative diffusivity* was scale-dependent. He found the diffusivity increased as the plume width to the four-thirds power, a relation now known as Richardson's Law.

Obhukov (1941) and Batchelor (1950) demonstrated that Richardson's Law was consistent with Kolmogorov's (1941) turbulence theory. Thus turbulent mixing in the planetary boundary layer could account for the smoke dispersion observed by Richardson. Numerous theoretical and experimental studies followed, particularly with regards to pollutants in the atmosphere (e.g. Frenkiel and Katz, 1956; Gifford, 1957). Excellent reviews are given by Bennett (1987, 2006) and Sawford (2001). In the spirit of the present review, we focus on the statistics of continuously tracked instruments in the ocean. We begin by establishing the terminology.

### 3.1. Theory

The following derivations follow those of Batchelor (1950, 1952a), Bennett (1984, 1987, 2006) and Babiano et al. (1990). We present the derivations for completeness, and for comparison with the single particle measures of Section 2.1.

The probability that two particles with an initial position of $x_0$ and separation $y_0$ will have a position $x$ and separation $y$ at a later time, $t$, depends on a joint displacement PDF:

$$P(x,y,t) = P(x_0,y_0,t_0)\mathcal{Q}(x,y,t|x_0,y_0,t_0)\mathrm{d}x_0\mathrm{d}y_0. \tag{39}$$

If we integrate $\mathcal{Q}$ only over the initial separations, $y_0$, we recover the single particle displacement PDF, $Q(x,t|x_0,t_0)$ (Section 2). If we integrate instead over the initial positions, $x_0$, we obtain a PDF of particle separations:

$$q(y,t|y_0,t_0) = \int \mathcal{Q}(x,y,t|x_0,y_0,t_0)\mathrm{d}x_0. \tag{40}$$

Richardson (1926) called this the "distance–neighbour function". If the flow is homogeneous, $\mathcal{Q}$ is independent of the initial position and equivalent to $q$. With the separation PDF, one can evaluate the probability of observing a given separation:

$$p(y,t) = \int p(y_0,t_0)q(y,t|y_0,t_0)\mathrm{d}y_0. \tag{41}$$

This can in turn be used to define moments. For example, the relative dispersion is

$$\overline{y^2}(t) = \int y^2 p(y,t)\mathrm{d}y. \tag{42}$$

We can also define the relative diffusivity:

$$K \equiv \frac{1}{2}\frac{\mathrm{d}}{\mathrm{d}t}\overline{y^2} = \overline{yv} = \overline{y_0 v} + \int_{t_0}^{t} \overline{v(t)v(\tau)}\mathrm{d}\tau, \tag{43}$$

where $v$ is the pair separation velocity. As the absolute diffusivity derives from the velocity autocorrelation, the relative diffusivity comes from the two particle velocity cross-correlation. However, because the separation velocity, $v$, usually varies with separation, we cannot factor out a mean square separation velocity from the integral.

There is an additional term in (43) which represents the correlation between the pairs' initial positions and their separation velocities. The integral of the autocorrelation dominates only after this correlation, the "memory" of the initial state, has been lost (Babiano et al., 1990). In principle this is zero, if the floats have been deployed randomly, but with pairs already present in the flow (hereafter called "chance pairs"), it may not be.

As before, we can infer the early and late time behavior from (43). If two particles are very close, their velocity difference is approximately constant. Then the separation distance increases linearly in time, as does the relative diffusivity. When the particle separations are larger than the size of the dominant eddies, the individual velocities are uncorrelated. Then, assuming the integral in (43) converges, the relative diffusivity is constant. Moreover, it is equal to twice the absolute diffusivity, because the mean square separation velocity:

$$\overline{v^2}(t) = \overline{(u_i(t) - u_j(t))^2} = 2v^2 - 2\overline{u_i u_j} \tag{44}$$

is just twice mean square single particle velocity if the individual velocities are uncorrelated. Thus relative dispersion behaves like absolute dispersion at small and large scales.

At intermediate scales the pair velocities are correlated and the dispersion depends on the flow. Consider a two-dimensional turbulent flow with stationary statistics (Bennett, 1984). If the flow is homogeneous, the Lagrangian velocity difference is the same as the Eulerian difference:

$$\overline{v(y)^2} = \overline{(u(x+y,t) - u(x,t))^2} = 2\int_0^\infty E(k)[1 - J_0(ky)]\mathrm{d}k \tag{45}$$

where $E(k)$ is the Eulerian wavenumber spectrum and $J_0$ is the first Bessel function. At the scales larger than the separation, we have

$$1 - J_0(ky) \approx \frac{1}{4}k^2y^2, \quad ky \ll 1, \tag{46}$$

while at the smaller scales

$$1 - J_0(ky) \approx 1 + \mathrm{O}(ky)^{-1/2}, \quad ky \gg 1. \tag{47}$$

Assuming the Eulerian spectrum has a power law dependence, $E(k) \propto k^{-\alpha}$, then

$$\overline{v(y)^2} \approx 2\int_0^{1/y} k^{-\alpha}\left(\frac{1}{4}k^2y^2\right)\mathrm{d}k + 2\int_{1/y}^\infty k^{-\alpha}\mathrm{d}k \tag{48}$$

or

$$\overline{v(y)^2} = \frac{1}{2}y^2\frac{1}{3-\alpha}k^{3-\alpha}|_0^{1/y} + \frac{2}{1-\alpha}k^{1-\alpha}|_{1/y}^{\infty} \tag{49}$$

The first term diverges if $\alpha \geqslant 3$ (steep spectra) while the second diverges if $\alpha \leqslant 1$. For intermediate values, when $1 < \alpha < 3$:

$$\overline{v(y)^2} \propto y^{\alpha-1}. \tag{50}$$

The corresponding diffusivity can be shown to scale as (Bennett, 1984)

$$K = \frac{1}{2}\frac{\mathrm{d}}{\mathrm{d}t}\overline{y^2} \propto y^{(\alpha+1)/2}. \tag{51}$$

So the diffusivity's dependence on separation directly reflects the slope of the energy spectrum. This is called "local dispersion", because the dispersion of pairs with separation $L$ is dominated by eddies of the same scale. Richardson's Law is an example of local dispersion.

For steep spectra ($\alpha \geqslant 3$), the relative dispersion is "non-local" and dominated by the largest eddies. From (48)

$$\overline{v(y)^2} \approx \frac{1}{2}y^2\int k^2E(k)\mathrm{d}k = c_1\Omega y^2, \tag{52}$$

where $c_1$ is a constant and $\Omega$ is the total enstrophy (the integrated square vorticity). The corresponding diffusivity is

$$K = \frac{1}{2}\frac{\mathrm{d}}{\mathrm{d}t}\overline{y^2} = c_2T^{-1}\overline{y^2}, \tag{53}$$

where $T$ is a time scale, proportional to the inverse root of the enstrophy. Relation (53) implies an *exponential growth* of pair separations. Exponential growth is a signature of Lagrangian chaos (e.g. Lichtenberg and Lieberman, 1992), as noted earlier. It is also found if one assumes small separations and a constant strain (as Batchelor (1952b) demonstrated for relative dispersion in the 3-D turbulent dissipation range). Then $T$ is proportional to the strain. Here we see that exponential growth occurs for all spectra steeper than $\alpha = 3$, so that observing exponential growth does not imply a single spectrum (Bennett, 1984; Babiano et al., 1990).

It is also useful to consider the pair displacement PDF. Richardson (1926) proposed this should obey a Fokker–Planck equation:

$$\frac{\partial}{\partial t}p(y,t) = y^{-1}\frac{\partial}{\partial y}\left(yK\frac{\partial}{\partial y}p\right), \tag{54}$$

where again $K = K(y)$ is the relative diffusivity. The same relation was derived analytically by Kraichnan (1966) and Lundgren (1981). With (54), one can predict the evolution of the separation PDF in time. For example, under local dispersion the separation kurtosis (Section 1.2) is constant, and has a value which depends on the energy spectral slope, $\alpha$ (Bennett, 1984). In contrast, the kurtosis grows exponentially under non-local dispersion. Therefore a second signature of non-local dispersion is that the PDFs become increasingly non-Gaussian with time (the PDF in Fig. 2 is an example from non-local dispersion). Stochastic dispersion yields a Gaussian distribution, and we often observe that the PDF becomes Gaussian when the pair velocities are uncorrelated.

### 3.1.1. Turbulent dispersion

Turbulence is frequently used as a paradigm for relative dispersion in the atmosphere and ocean. At small scales, and in particular in the planetary and surface boundary layers, the turbulence is three dimensional. Energy in the turbulent inertial range cascades at a constant rate across wavenumbers, yielding a spectrum with a $\kappa^{-5/3}$ dependence (Kolmogorov, 1941; Batchelor, 1953). At synoptic scales, the flow is more nearly two dimensional, due to the suppression of vertical motion by rotation and stratification. Energy also cascades at a constant rate in 2-D turbulence, but toward larger rather than smaller scales. However, the same spectral slope of $\kappa^{-5/3}$ is found (Kraichnan, 1967). So in the energy inertial range in either 2-D or 3-D turbulence, we have

$$\overline{y^2} \propto \epsilon t^3, \quad K \propto \epsilon^{1/3}y^{4/3}, \quad ku(y) = \text{Const.}, \tag{55}$$

where $\epsilon$ is the (constant) energy dissipation rate (with units of $L^2/T^3$). As noted earlier, the 4/3 dependence for the diffusivity is as predicted by Richardson (1926).

Two-dimensional turbulence exhibits a second inertial range, in which the enstrophy (the squared vorticity) cascades to smaller scales. Here the spectrum has $\kappa^{-3}$ dependence (Kraichnan, 1967; Charney, 1971), so the pair separations grow exponentially in time (Lin, 1972):

$$\overline{y^2} \propto \exp(c_3\eta^{1/3}t), \quad K \propto \overline{y^2}, \quad ku(y) \propto \exp(c_4\eta^{1/3}t), \tag{56}$$

where $\eta$ is the enstrophy dissipation rate (with units of $1/T^3$).

What one observes with 2-D turbulence therefore depends on which cascade is occurring at the scale of the pair's separation. Consider a pair with an initial separation much smaller than the scale at which the energy is injected (Fig. 15). This scale might be the deformation radius, in the presence of baroclinic instability (Salmon, 1980). The relative dispersion would grow exponentially in time until it reached the injection scale, and thereafter it would increase cubically in time, up to the scale of the largest eddies.

### 3.1.2. Shear dispersion

Just as absolute dispersion is affected by a constant background flow, relative dispersion is affected by background shear. For example, a constant shear, $U(y)$, will cause *ballistic* relative dispersion in the $x$-direction:

$$\langle[x_i - x_j]^2\rangle = \langle[U(y_i) - U(y_j)]^2\rangle t^2. \tag{57}$$

Consider that there is stochastic motion in addition to the shear (due for example to small scale eddies). For simplicity, take this to be a zeroth-order stochastic process in which the random motion occurs only across the shear (Bennett, 1987):

$$\begin{aligned}\mathrm{d}y &= \mathscr{K}^{1/2}\mathrm{d}w,\\ \mathrm{d}x &= \gamma y\mathrm{d}t\end{aligned} \tag{58}$$

where $\gamma = \mathrm{d}U/\mathrm{d}y$ is the meridional shear and $\mathscr{K}$ the meridional diffusivity. This yields

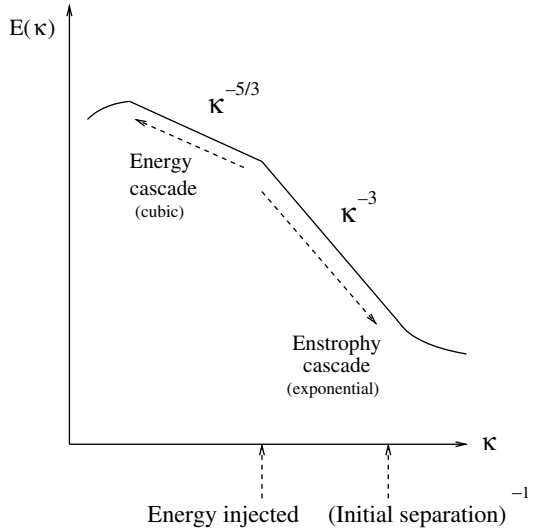


**Fig. 15.** The energy spectrum for two dimensional turbulence driven by a source at an intermediate scale. The enstrophy cascades to small scales, where it is dissipated, and the energy cascades to large scales. A particle pair with the initial separation shown will experience both growth regimes.

$$\langle y^2\rangle = 2\mathscr{K}t, \quad \langle xy\rangle = \mathscr{K}\gamma t^2,$$
$$\langle x^2\rangle = x_0^2 + \frac{2}{3}\mathscr{K}\gamma^2 t^3. \tag{59}$$

Because the pair velocities are uncorrelated, relative dispersion is like the absolute dispersion and both increase as $t^3$ (Bowden, 1965; Riley and Corrsin, 1974; Bennett, 1987; Zambianchi and Griffa, 1994). In addition, the cross-correlation is non-zero and increases quadratically in time.

Thus shear dispersion produces Richardson-type growth, exactly as in a turbulent cascade. What distinguishes this case is that the pair velocities are uncorrelated, so that the displacement PDF would be Gaussian.

### 3.1.3. FSLE

The standard procedure for computing relative dispersion is to average separations between available pairs at fixed times. This necessarily involves averaging pairs with different separations. However, this can be problematic, particularly under local dispersion where the dispersion is controlled by eddies comparable in scale to the separation.

An alternate approach is to use distance as the independent variable and average *times*. This is the idea behind the "finite scale Lyapunov exponent" (Aurell et al., 1997; Artale et al., 1997). In this, one selects a set of distances, increasing multiplicatively, i.e.:

$$d_n = rd_{n-1} = r^n d_0. \tag{60}$$

One then records the time required for individual pair separations to increase from one distance to the next. These "exit times" are then averaged.

The FSLE is related to the Lyapunov exponent, a measure used to characterize chaotic systems. As noted, Lagrangian chaos entails an exponential growth of the separation between two nearby particles. The maximum Lyapunov exponent reflects that growth rate:

$$\lambda = \lim_{t\to\infty}\lim_{y(0)\to 0}\frac{1}{t}\ln(\overline{y(t)}/\overline{y(0)}) \tag{61}$$

(Lichtenberg and Lieberman, 1992). Chaos implies that $\lambda > 0$. Under exponential growth, the exit times with multiplicatively increasing bin sizes is constant, so the mean inverse exit time is related to the growth rate:

$$\lambda = \frac{1}{\langle T_n\rangle}\ln(r). \tag{62}$$

This defines the FSLE.

The FSLE can also be used in cases without exponential growth. Then the exit times will not be constant but will vary with separation. If the dispersion has a power law dependence on time, as under local dispersion, the FLSE exhibits a power law dependence on separation. If the dispersion varies as

$$y^2 \propto t^\alpha \tag{63}$$

then the FSLE, as a mean inverse time, scales as

$$\lambda \propto y^{-2/\alpha}. \tag{64}$$

So growth in the Richardson regime has an FSLE which decreases as the separation to the minus two-thirds power.

In some numerical simulations, the FSLE yields a clearer indication of scale dependence in the Richardson regime (Boffetta and Celani, 2000). The FSLE also uses all available pairs, not just those deployed together, and this can increase the degrees of freedom. However, the FSLE does have several shortcomings with regards to in situ data, as discussed hereafter.

## 3.2. Relative dispersion in the atmosphere

While we are primarily concerned with oceanic results, it is useful to examine the results of two important atmospheric studies. These were conducted in the southern hemisphere stratosphere during the 1970s: the EOLE experiment (with 483 constant level balloons, at 200 mb; Morel and Bandeen, 1973) and the TWERLE experiment (with 393 constant level balloons at 150 mb; Jullian et al., 1977). In both cases, balloons were launched in pairs or clusters. The relative dispersion in these experiments was described in two seminal papers, by Morel and Larcheveque (1974) and by Er-el and Peskin (1981).

Pair statistics in general require larger numbers of realizations for statistical convergence, so Morel and Larcheveque increased their sample size by using chance pairs (balloons which were not deployed together but drifted near one another at a time later). As noted earlier, this is potentially problematic because the separations are more likely to be correlated with the separation velocities (Section 3.1). But Morel and Larcheveque found that statistics derived from the chance pairs were identical to those from deployed pairs.

The relative dispersion for the EOLE pairs is plotted in Fig. 16. The growth is very nearly exponential over roughly the first 6 days, with an e-folding time scale of 1.35 days. The exponential growth persists to a scale of about 1000 km, and grows linearly in time at larger scales. Were the atmosphere a 2-D turbulent fluid, we might infer an enstrophy cascade below a dominant eddy scale of 1000 km. However, as stated earlier, exponential growth does not necessarily imply an enstrophy cascade; any spectrum steeper than $\kappa^{-3}$ will also cause exponential growth.

Er-el and Peskin (1981) obtained similar statistics at small scales with the TWERLE balloons (Fig. 17). The relative dispersion exhibited exponential growth below 1000 km, during the first week after deployment (or the initialization of chance pairs, which they also used). At large scales however, the dispersion increased more rapidly than linearly in time. A $t^3$ dependence was possible, suggestive of an inverse energy cascade (the scales being too large for 3-D turbulence). As 1000 km is comparable to the deformation radius, the implied behavior would thus be like that discussed in relation to Fig. 15. However, the statistics at large scales were noisy, so that other dependences could not be ruled out.

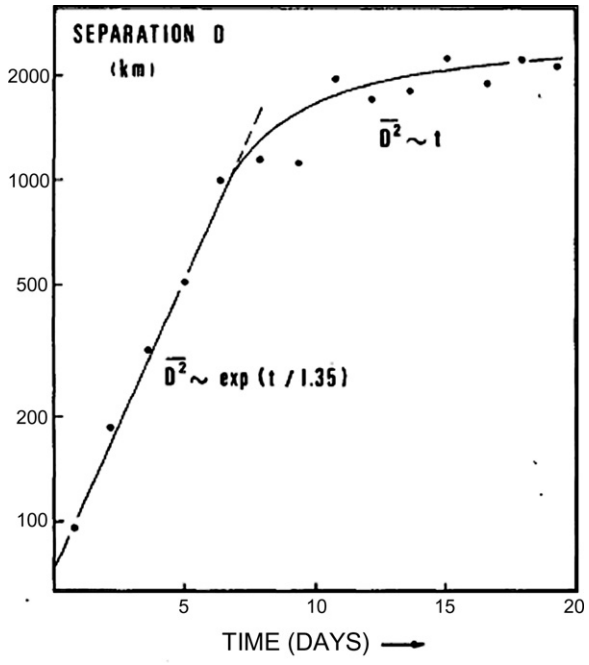


**Fig. 16.** Dispersion vs. time for the EOLE balloon pairs. From Morel and Larcheveque (1974), with permission.

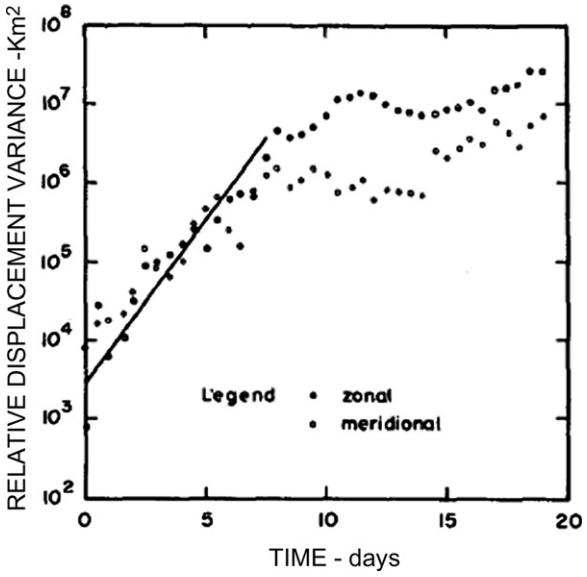


**Fig. 17.** The PDF of relative zonal displacements 5 days after deployment from the TWERLE balloons. From Er-el and Peskin (1981), with permission.

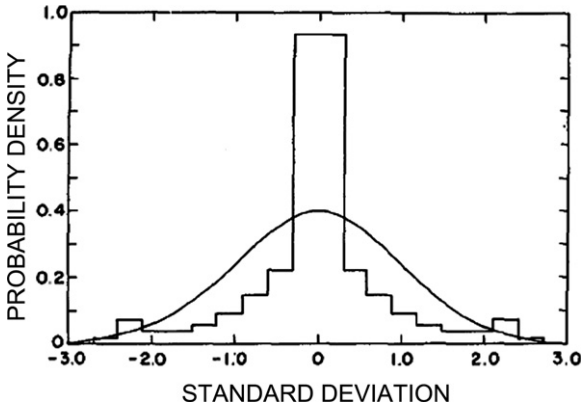


**Fig. 18.** Relative dispersion vs. time for the TWERLE balloons. From Er-el and Peskin (1981).

In both studies, the dispersion was approximately isotropic below 1000 km (in the exponential growth range) but preferentially zonal at larger scales. The latter may come from the mean circulation, which is also primarily zonal. If so, the rapid later growth described by Er-el and Peskin (1981) might reflect shear dispersion (Section 3.1.2).

Er-el and Peskin also calculated PDFs of the pair separations, during the exponential growth phase (Fig. 18). The kurtoses in the zonal/meridional direction were 7.5/7.0, indicating significantly non-Gaussian distributions. This is consistent with non-local dispersion (Section 3.1). However, because Er-el and Peskin calculated the PDF at only one time, we don't know whether the kurtosis was increasing.

The existence of an exponential growth range was questioned recently by Lacorata et al. (2004), who re-examined the EOLE data set using the FSLE (Section 3.1.3). Their results suggest a power law rather than exponential growth below 500–1000 km, with a scale dependence consistent with the Richardson law. If correct, this would agree better with energy spectra in the upper troposphere, which indicate a $\kappa^{-5/3}$ dependence at these scales.

Other analyses (using models and/or reanalysis winds) suggest the dispersion may vary with height and also with latitude. Tracer transport studies suggest that stirring in the stratosphere is dominated by large scale, low frequency motions, such as Rossby waves. Such stirring would produce exponential growth at small scales. In the mesosphere, gravity waves cause the energy spectra to be shallower and the dispersion is therefore local (Shepherd et al., 2000). Studies of relative dispersion in the troposphere suggest that exponential growth occurs in the tropics, while the dispersion in the extra-tropics is nearly ballistic (Huber et al., 2001).

In summary, both the EOLE and TWERLE studies indicated exponential growth in pair separations below the 1000 km scale. The large scale behavior was unclear, with the EOLE data indicating diffusive growth and the TWERLE data showing a power law. The results also suggested isotropic dispersion at small scales and zonally enhanced spreading at larger scales, as well as non-Gaussian separation distributions at the small scales. Nevertheless, the overall picture remains unsettled, with recent analyses suggesting different, and possibly regionally varying, dispersion.

### 3.3. Relative dispersion in the ocean

The origins of relative dispersion experiments in the ocean are colorful. Intrigued by Richardson's work, Henry Stommel visited the scientist in England and the two subsequently conducted a pair dispersion experiment at the surface of Loch Long in Scotland. For this they used pairs of parsnip pieces[9] and monitored the growth of separations visually. The results supported Richardson's law over the range of sampled scales (Richardson and Stommel, 1948). As quaint as it sounds, it nevertheless was a *particle*-based study, in contrast to Richardson's earlier work which concerned a continuous tracer (smoke). Stommel (1949) described further experiments (using other objects, like paper cards) and also discussed the connection to Kolmogorov's (1941) theory.

Okubo (1971) and Sullivan (1971) also examined surface dispersion, based on dye releases in the North Sea and on Lake Huron, respectively. Okubo's results in particular spanned a large range of horizontal scales (from 10 m to 100 km). The results in both cases supported the Richardson scaling. Sullivan (1971) also examined the relative displacement PDFs (the first to do so), to compare two different predictions due to Richardson (1926) and Batchelor (1952a). A later dye-based experiment, by Anikiev et al. (1985), lent further support to the Richardson scaling at the ocean surface.

Kirwan et al. (1978) analyzed pair dispersion among continuously tracked surface drifters, in the North Pacific. The primary result of their analysis was an apparent transition from relative to absolute dispersion at the 50–100 km scale. This implies that the energy-containing eddies were of comparable size, or approximately deformation scale.[10] They did not however examine the dependence of the diffusivity on distance at smaller scales.

Davis (1985) examined pair statistics from continuously tracked surface drifters in the California Current. He found no consistent dependence of the diffusivity on distance. In addition, the dispersion had different characteristics in different regions, which he attributed to small scale convergences in the surface flow. Davis also calculated the separation PDFs and found they were non-Gaussian soon after deployment. The PDFs at larger separations were Gaussian, suggesting a shift from correlated to uncorrelated pair velocities.

[9] As noted by the authors, parsnips are easily visible and float just below the surface, reducing wind drag. In a further note, they lamented the necessity of observing from a pier because of interference from the support posts. "A suspension bridge would have been an ideal platform", they suggested.

[10] Consistent with this, Stammer (1997) finds that the dominant eddy scale at the ocean surface is proportional to the deformation radius.

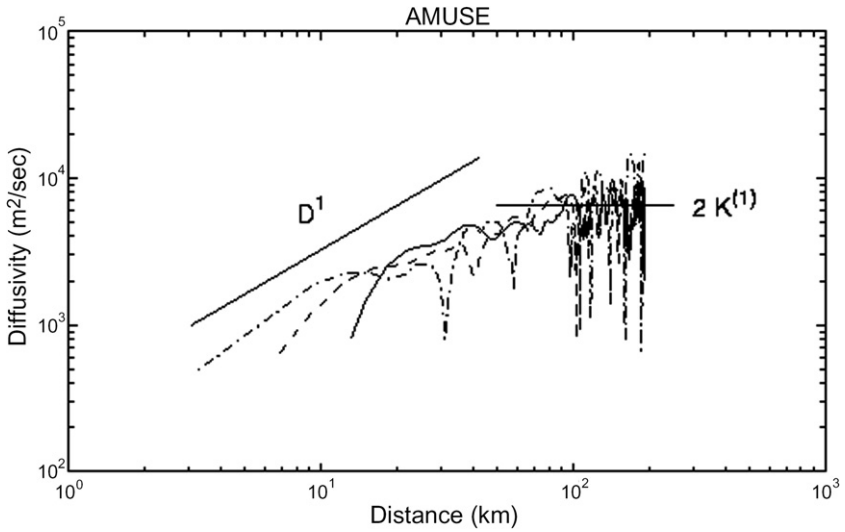


**Fig. 19a.** Relative diffusivity vs. distance for floats in the eastern North Atlantic. The three curves correspond to initial pair separations of 7.5, 15 and 30 km. The horizontal line indicates twice the absolute diffusivity.

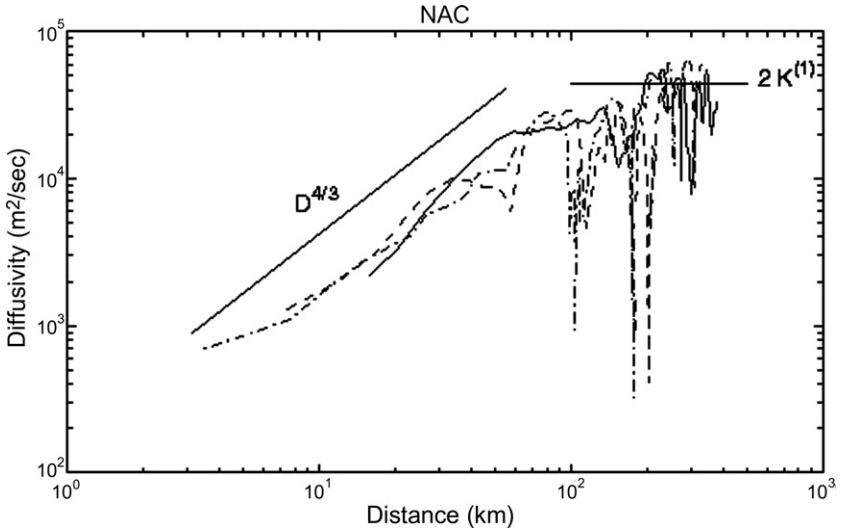


**Fig. 19b.** Relative diffusivity vs. distance for floats from the western North Atlantic, with initial separations of 7.5, 15 and 30 km. From LaCasce and Bower (2000).

One of the earliest relative dispersion analyses with continuously tracked floats was by Price (in McWilliams et al., 1983) from SOFAR floats in the recirculation south of the Gulf Stream. Plotting relative diffusivity vs. distance, he found a power law dependence on scales of less than a few hundred kilometers. The slope was such that $K \propto y^n$ with $4/3 \leqslant n \leqslant 2$, consistent with either a Richardson regime or exponential growth.[11]

LaCasce and Bower (2000) examined subsurface relative dispersion using different SOFAR and RAFOS float data from the North Atlantic (of which Price's floats were a subset). In most cases the floats had not been deployed in pairs, so the authors had to rely on chance pairs. There were relatively few pairs with small initial separations (with $y_0 < 10$ km), but several features were apparent.

For one, the relative dispersion was isotropic, in all regions and at all scales. This was true whether the absolute dispersion was isotropic or not. However, the dispersion in the eastern Atlantic differed from that in the west. In the east, there was no evidence for correlated pair velocities at *any* of the sampled scales, so that the relative dispersion behaved like absolute dispersion (Fig. 19a). Evidently, the initial pair separations were not small enough relative to the energy-containing eddy scale. As with Kirwan et al. (1978) Pacific drifters, the transition to a constant diffusivity occurred at about 50 km.

In contrast, the pair velocities in the western Atlantic were correlated for separations up to 100–200 km, and the relative dispersion increased more rapidly than linearly with distance. The data, though noisy, suggested a $y^{4/3}$ dependence (Fig. 19b). This result was thus consistent with the lower estimate of Price's. The relative diffusivity at scales larger than 200 km was approximately constant.

LaCasce and Bower also examined the relative displacement PDFs, and plotted their evolution in time. Plotted in Fig. 20 is the displacement kurtosis for the five data sets examined. The two sets from the eastern and central Atlantic (AMUSE and ACCE) have kurtoses near three for the entire period, indicating Gaussian distributions. In contrast the three western sets (NAC, SiteL, LDE1300) exhibit a rapid growth followed by a 20–30 days period in which

[11] The number of float pairs was fairly small and Price was uncomfortable with asserting a particular dependence (Price, pers. comm.).

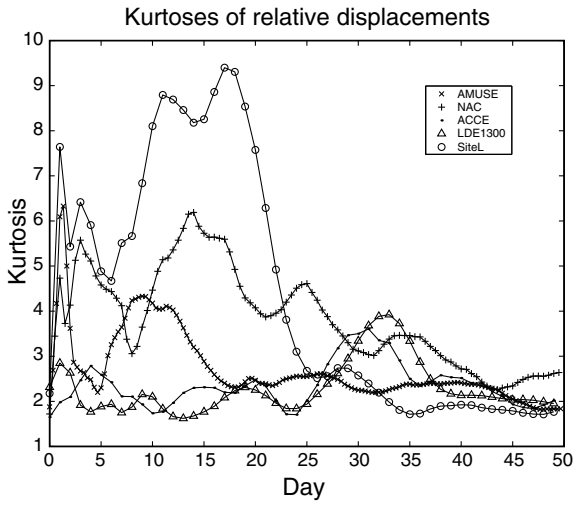


**Fig. 20.** Relative displacement kurtoses vs. time for the five float experiments examined by LaCasce and Bower (2000). The AMUSE and ACCE experiments were in the eastern and central North Atlantic, while the NAC, LDE and SiteL experiments were in the west. The latter three exhibit non-Gaussian kurtoses during the first 20 days. From LaCasce and Bower (2000).

the kurtoses were elevated. At late times the kurtoses fall back toward three. Taken together with the dispersion plots, this would imply correlated pair velocities up to roughly 100 km.

There are at least two possible explanations for Richardson-type dispersion in the west. One is that an inverse energy cascade is occurring in the Gulf Stream region, from the deformation scale (roughly 30 km) up to 200 km. The cascade could conceivably be driven by baroclinic instability, as discussed in Section 3.1.1. Indeed, Scott and Wang (2005) inferred such an upscale energy transfer from the deformation radius at the surface in the South Pacific, from satellite altimeter data.

Alternately, the growth could reflect shear dispersion due to the Gulf Stream. Indeed, the Gulf Stream dominates the flow where the most of the western floats are. However, if it is shear dispersion, it is a somewhat different process than described in Section 3.1.2. For one, the pair velocities were correlated (LaCasce and Bower, 2000). The dispersion moreover is isotropic, and the cross-correlation between the zonal and meridional separations is zero. So the process is more complex than stochastic motion in the presence of a fixed shear.

Ollitrault et al. (2005) presented a detailed analysis of pair dispersion using floats deployed in the central North Atlantic. Their results (Fig. 21) suggest a Richardson regime up to 200–300 km in both the western and eastern Atlantic. They also found support for exponential growth below the deformation radius (30 km) in the eastern basin, with an e-folding time scale of 12 days (similar to an estimate derived from idealized model simulations by Berloff et al., 2002). At the largest scales, the relative diffusivity asymptoted to twice the absolute diffusivity, as expected for uncorrelated pairs.

The authors also calculated separation PDFs. These were non-Gaussian for pairs with initial separations less than 10 km, but Gaussian for pairs with separations in the range 30–40 km (exactly as Davis (1985) found with his drifters in the California Current). Consistent with this, the rms relative velocities suggested correlated motion at early times, or up to roughly 50 km, and uncorrelated velocities at larger scales. The latter would favor a shear dispersion interpretation of the observed Richardson growth rather than an inverse cascade. However the authors argued for the latter, because the late dispersion was isotropic. Thus the situation described by Ollitrault et al. (2005) is very like that of the western floats of LaCasce and Bower (2000).

It was difficult to resolve the sub-deformation scale dispersion in these studies, in part because the deformation radius at these latitudes is only about 30 km. However these scales were better resolved in the SCULP program in the Gulf Mexico (Ohlmann and Niiler, 2005). This involved roughly 700 surface drifters, many of which were deployed near one another. The result was 140 pairs with initial separations $r_0 \leqslant 1$ km, the largest such set in an ocean experiment to date. In addition, the deformation radius is roughly 45 km in the Gulf, sufficiently larger than the 1 km separation.

The SCULP relative dispersion is shown in Fig. 22a. There is exponential growth to roughly 50 km, over the first 10 days of the pair lifetimes, with an e-folding time of roughly 2 days. The dispersion during this period is also isotropic. Thus the dispersion resembles that at sub-deformation scales in the EOLE and TWERLE experiments in the stratosphere (Section 3.2). The dispersion at late times is consistent with a power law growth, i.e. $D^2 \propto t^n$ (Fig. 22b). The exponent, $n \approx 2.2$, is less than expected for a Rich-

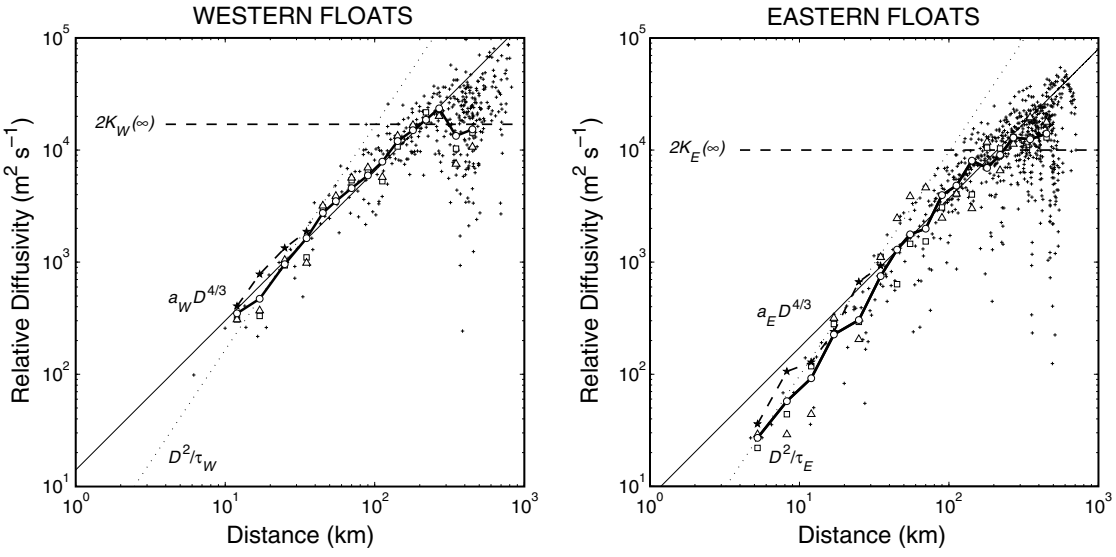


**Fig. 21.** Relative diffusivity vs. distance for the subsurface floats in the central North Atlantic. The various symbols correspond to different initial separations. The solid curve with the open circles indicates the averages in distance bins. The solid and dotted lines indicate a Richardson and an exponential growth scaling, respectively. From Ollitrault et al. (2005), with permission.

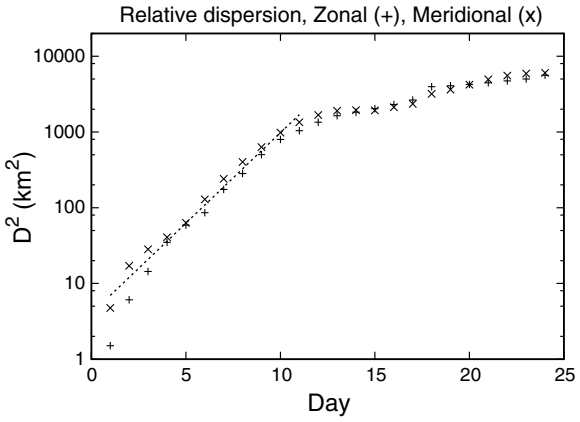


**Fig. 22a.** Relative dispersion vs. time for surface drifters in the SCULP experiment in the Gulf of Mexico. The zonal dispersion is indicated by the ×-curve and the meridional by the +-curve. The dashed line indicates exponential growth with a e-folding time scale of 1.8 days.

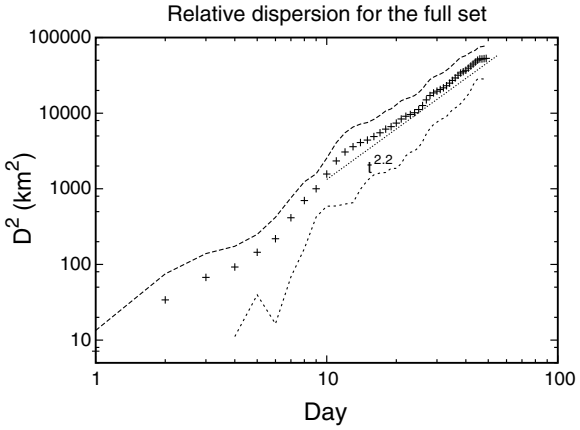


**Fig. 22b.** The total relative dispersion at late times. The straight line indicates a power law growth with a best-fit slope of 2.2, and the dashed lines indicate the error estimates. From LaCasce and Ohlmann (2003).

ardson regime, but cubic growth cannot be ruled out given the errors. The result in any case suggests local dispersion.

The displacement kurtoses (Fig. 23) indicate highly non-Gaussian distributions over the first 3 days, and persistent non-Gaussianity over the first 25 days. The rapid growth in the first few days is what one would expect with non-local dispersion (Section 3.1), however the rapid decrease seen in days 4–6 and the relatively constant kurtosis from days 5 to 20 is not expected for non-local dispersion. In addition, the kurtoses are *anisotropic*, with larger values in the meridional direction. This is striking, as the dispersion is isotropic. The anisotropy may reflect the influence of the similarly oriented boundary current in the western Gulf. The meridional kurtosis remains non-Gaussian until day 40, long after the zonal kurtosis has relaxed to three. So it remains unclear how these kurtoses relate to the relative dispersion.

As in the previous examples, the late time power law growth could reflect either a Richardson regime or shear dispersion. Some indications favor the shear interpretation (the pair velocities at late times are decorrelated) while others favor a Richardson regime (the behavior of triplets, described below). The dispersion however never settles into a diffusive stage; the power law growth persists to the largest sampled scales (of several hundreds of kilometers).

An important caveat is that the ocean surface is divergent. Because drifters remain at the surface, they cannot track the vertical motion of fluid parcels. The result is that drifters collect at convergences, and this can alter the dispersion (e.g. Schumacher and Eckhardt, 2002). Thus interpreting dispersion with drifters is not as straightforward as with the floats, where divergence effects are much less. We consider divergence effects further in Section 3.4.

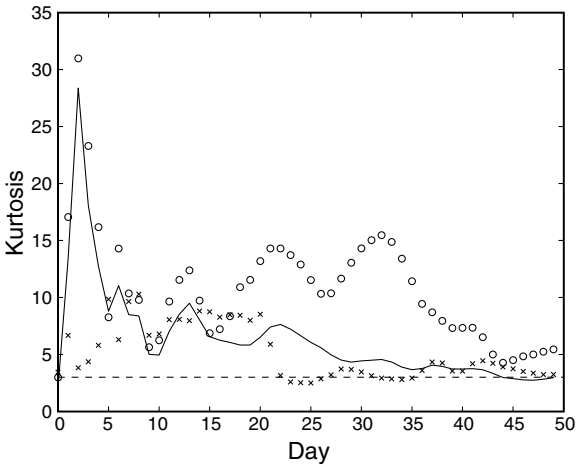


**Fig. 23.** The kurtosis of the relative displacements as functions of time. The solid line is for the total displacements and the circles/crosses are for the meridional/zonal displacements. The Gaussian value of three is indicated by the dashed line. From LaCasce and Ohlmann (2003).

Several studies also used the FSLE to measure the dispersion. LaCasce and Bower (2000) did so using the North Atlantic float data, but the results were inconclusive. From the dispersion, we would expect the mean inverse time to vary as $y^{-2}$ in the east and $y^{-2/3}$ in the west. However, while all the data sets indicated a decrease in the mean inverse time with separation, no clear power law dependence was found. At best, the decrease in the west was less rapid than in the east.

Lacorata et al. (2001) were more successful, in a study of surface dispersion in the Adriatic. They calculated the FSLE using trajectories from 37 in situ drifters and $10^4$ synthetic drifters, the latter coming from a idealized kinematic model. The results (Fig. 24) suggested two regimes with a constant FSLE, at scales less than 50 km and greater than 100 km. The growth would be exponential in both cases, with doubling times of 3 and 30 days respectively. What is interesting is that they obtained nearly the same behavior with the kinematic model, despite its drastic simplifications.

LaCasce and Ohlmann (2003) also calculated the FSLE, for comparison with their relative dispersion. This also indicated two regimes. The FSLE was approximately constant at scales less than 10 km, with an e-folding time of about 3 days, while at larger scales there was a $y^{-2/3}$ dependence, consistent with the Richardson scaling. The FSLE thus agreed with relative dispersion at small scales and indicated a Richardson scaling at large scales.

There are however important discrepancies with the relative dispersion. For one, the transition between the early and late phases occurs at 10 km for the FSLE but nearer 50 km for the relative dispersion. The authors suggested this difference stemmed from the FSLE using pairs with too large separations. By calculating the FSLE with only the pairs with an initial separation of 1 km, they obtained roughly the same transition scale (50 km). So the pairs with larger initial separations, in the 1–10 km range, may not have reached the asymptotic exponential growth period.

There is another difference though, overlooked by the authors. Because the FSLE involves distance, not distance squared, the e-folding time for the dispersion implied by the FSLE is actually 6 days, three times larger than the estimate from relative dispersion. It turns out that this discrepancy stems from insufficient temporal resolution of the data (1 day).

If the resolution is too coarse, the fast-separating pairs are incorrectly represented in the average. For instance, if a given pair

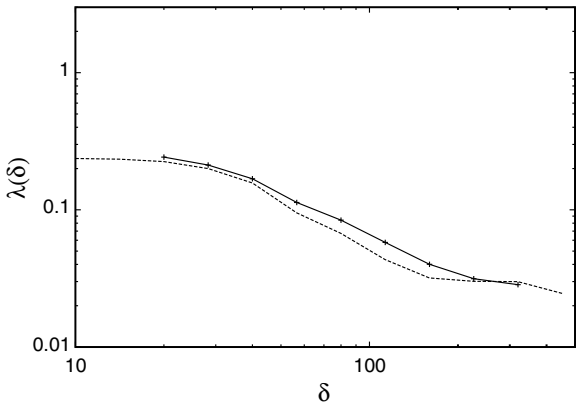


**Fig. 24.** The FSLE plotted against separation (in km) using data from 37 surface drifters (dotted solid line) and from $10^4$ synthetic drifters (dashed line) in the Adriatic. From Lacorata et al. (2001), with permission.

requires only half a day to separate from 1 to 2 km, that exit time would be misrepresented in the average. To test this, we interpolated the SCULP pair separation time series to finer resolution (1/5, 1/10 and 1/20 of a day). As seen in Fig. 25, increasing the temporal resolution does indeed shift the small scale plateau to larger inverse times. The curves converge at the highest resolutions, where the doubling time is comparable to that inferred from relative dispersion (roughly 0.9 day$^{-1}$). Including the fast separation times is thus critical to capture the small scale growth.

This conclusion is supported by a recent study in which the FSLE was calculated from synthetic data generated by a model of the Adriatic Sea (Haza et al., in press). The authors used the surface velocity fields to advect drifters, and tested how the FSLE changed if the model fields were filtered temporally or spatially. They demonstrated that coarse temporal resolution degrades the FSLE at small scales, producing a plateau with an artificially low growth rate, as seen here. In their case, the plateau vanishes altogether with sufficient temporal resolution, because most of the chance pairs were in boundary currents, experiencing shear dispersion. Using original pairs deployed throughout the domain, they recovered a plateau and hence exponential growth.

Relative dispersion is much more robust with regards to temporal resolution. Using the interpolated SCULP time series produces identical dispersion curves, just with finer spacing. Presumably the relative dispersion would suffer if the advecting velocities were smoothed spatially, but this is obviously not an issue with in situ data.

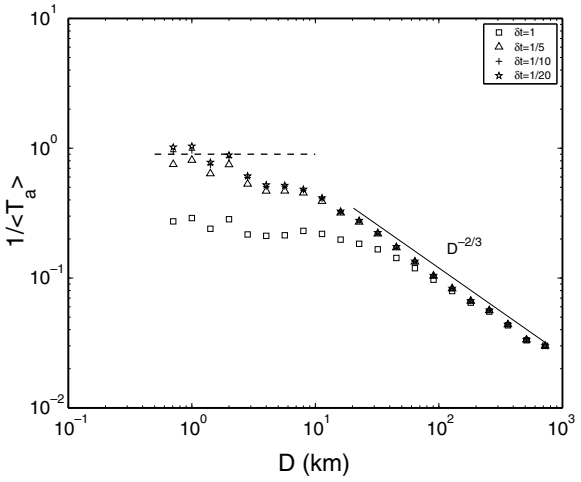


**Fig. 25.** The FSLE with the SCULP drifter data. The squares correspond to daily data, while the curves with triangles, pluses and stars derive from time series interpolated to one-fifth, one-tenth and one-twentieth of a day, respectively. The dashed line indicates the mean inverse exit time inferred from the relative dispersion.

On the other hand, the FSLE is relatively unaffected by the interpolation at the largest scales (Fig. 25). The only difference is that the higher resolution cases exhibit a transition to the power law decay at somewhat smaller separation scales, as the small distance plateau shifts to larger values. Surprisingly, the transition scale is not significantly different when using only the $r_0 = 1$ km pairs. So that result is also affected by the temporal resolution of the data.

Of course, this interpolation to finer resolution is artificial, because drifter time series with a time spacing of 1/20th of a day would include inertial oscillations (which were filtered out of the daily data). So the small scale behavior seen in Fig. 25 is likely very different in reality.

Thus the FSLE scaling at large scales agrees with that inferred from relative dispersion, within the errors. At small scales, however, the FSLE is sensitive to the temporal resolution of the data, particularly if the resolution is comparable to the e-folding time scale. This sensitivity is not an issue for model-generated trajectories, where the resolution is as fine as required. But it is relevant for in situ data.

### 3.4. Three or more particles

Using larger groups of particles can shed additional light on the dispersion. For instance, the folding of material lines can be detected with three particles (e.g. Thiffeault, 2005). Here we consider a number of studies involving three or more particles.

Consider a group of drifters at the ocean surface. If the drifters are close enough to each other, the material inside the polygon formed by them will be conserved, so that

$$\frac{1}{A}\frac{\mathrm{d}A}{\mathrm{d}t} = \left(\frac{\partial u}{\partial x} + \frac{\partial v}{\partial y}\right). \tag{65}$$

Thus one can diagnose surface divergence by monitoring changes in the cluster area.

This idea was explored by Molinari and Kirwan (1975) with drifters from the western Caribbean. The authors also used clusters to calculate vorticity, stretching and shearing deformations by using a clever transformation due to Saucier (1955). Saucier's method involves rotating the instantaneous velocity vectors of the constituent drifters. For instance, by replacing

$$u \to v', \quad v \to u'$$

one obtains for the vorticity:

$$\zeta = \frac{\partial v}{\partial x} - \frac{\partial u}{\partial y} = \frac{\partial u'}{\partial x} + \frac{\partial v'}{\partial y} = \frac{1}{A'}\frac{\mathrm{d}A'}{\mathrm{d}t},$$

if $A'$ is the area enclosed by the cluster with the vertices formed by the rotated velocity vectors. Similar transformations can be used to obtain the shearing and stretching terms.

Alternatively, one can calculate the same quantities by differencing drifter velocities (Molinari and Kirwan, 1975; Okubo and Ebbesmeyer, 1976; Okubo et al., 1976; Fahrbach et al., 1986; Niiler et al., 1989; Paduan and Niiler, 1990; Swenson et al., 1992). In this, one expands the velocities of the individual drifters in Taylor series about the velocity of the cluster center:

$$u_i = u_c + \frac{\partial u_c}{\partial x}(x_i - x_c) + \frac{\partial u_c}{\partial y}(y_i - y_c) + u_i', \tag{66}$$

$$v_i = v_c + \frac{\partial v_c}{\partial x}(x_i - x_c) + \frac{\partial v_c}{\partial y}(y_i - y_c) + v_i', \tag{67}$$

where $(u_c, v_c)$ and $(x_c, y_c)$ are the velocities and positions of the center. These equations can be used to estimate the shear terms using a least squares formulation. With four or more particles, one can also

obtain error estimates for the shears. The results improve with the number of particles, and Okubo and Ebbesmeyer (1976) suggested 6 would yield reasonable estimates. The results are also sensitive to the aspect ratio of the cluster; if it is too strained out, the estimates are degraded (Righi and Strub, 2001). The latter authors obtained accurate results with synthetic drifters in a 1/12th of a degree model of the California Current using clusters of 5. Molinari and Kirwan (1975), Niiler et al. (1989), Paduan and Niiler (1990) and Swenson et al. (1992) all obtained plausible results with groups of only 3 or 4 drifters.

Molinari and Kirwan (1975) moreover compared the area and center-of-mass methods and found they produced nearly identical results (Fig. 26). This supported the assumptions underlying both methods. As noted, the drifters must be close for this to work, and the rms separation in Molinari and Kirwan's groups was only a few kilometers. The vorticity estimates are of order $10^{-5}$ $s^{-1}$, indicating a Rossby number of order 0.1.

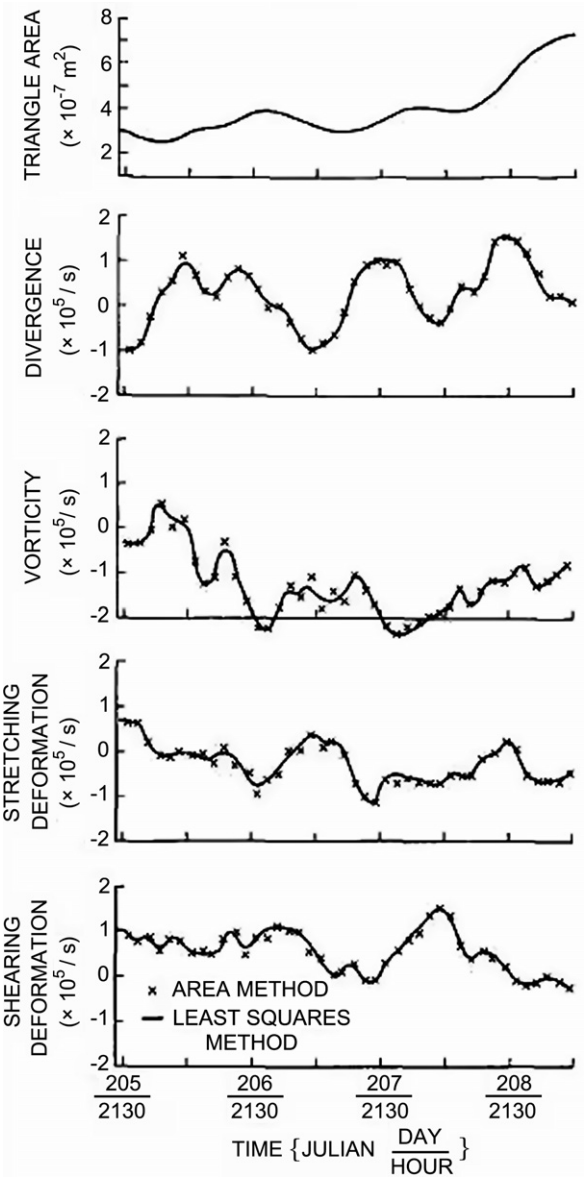


**Fig. 26.** An example of diagnostics calculated from a triplet of drifters by Molinari and Kirwan (1975). Shown are the area, divergence, vorticity, and the stretching and shearing deformations. The solid lines represent quantities derived using the least squares method and those derived by the area method by ×'s. Reproduced with permission.

Molinari and Kirwan went further and used the vorticity and divergence estimates to evaluate a Lagrangian vorticity balance for the drifter clusters:

$$\frac{d}{dt}(\zeta + f) + (\zeta + f)\left(\frac{\partial u}{\partial x} + \frac{\partial v}{\partial y}\right) = \text{resid.} \tag{68}$$

Although the residuals were comparable in size to the two terms on the LHS, there were clear indications that those terms were balancing each other.

Mariano and Rossby (1989) made similar calculations with data from SOFAR floats in the western Atlantic. These were deployed during the local dynamics experiment (LDE) at 700 and 1300 m. Below the surface, the flow is approximately three dimensionally non-divergent. However, vertical stretching can produce horizontal divergence, as in (68). Thus (68) still applies, but now the divergence reflects vortex stretching. It is difficult to estimate the divergence directly from the velocity shears because it involves the difference of two large terms (presumably because the velocities are nearly geostrophic). So they used several other methods to infer the stretching, one of which involved using hydrographic data from ships in the vicinity.

The results were limited, but suggested that all three terms were important. Moreover, it was often apparent that two of the terms were balancing when the third was small. They found that the 1300 m floats were clearly influenced by the topography, in a manner consistent with the mixed Rossby wave advection inferred by Price and Rossby (1982).

Now imagine that the divergence is weak, so that the area between three particles is approximately conserved. Then an exponential growth of the separation between two of the particles must be balanced by an equally rapid contraction in the distance perpendicular to the line joining them and the third particle. This was noted by Batchelor (1952b) in the context of dispersion in the presence of a constant strain, and by Garrett (1983) for the enstrophy cascade in 2-D turbulence.

Of course the ocean surface is divergent and area need not be conserved. But we can assume it is and examine the consequences. The SCULP drifters in the Gulf of Mexico were of sufficient density to yield a small number of "chance" triplets. One such, over the continental shelf, is shown in Fig. 27. The triangle was drawn out early on, collapsing nearly to a line. Later it grew, gradually returning to a isosceles triangular shape.

There were roughly 30 such triangles. The mean triangle base (defined as the longest leg) grew approximately exponentially in time during the first 10 days, at a rate consistent with the mean pair dispersion (Fig. 28). The triangle height is also increasing,

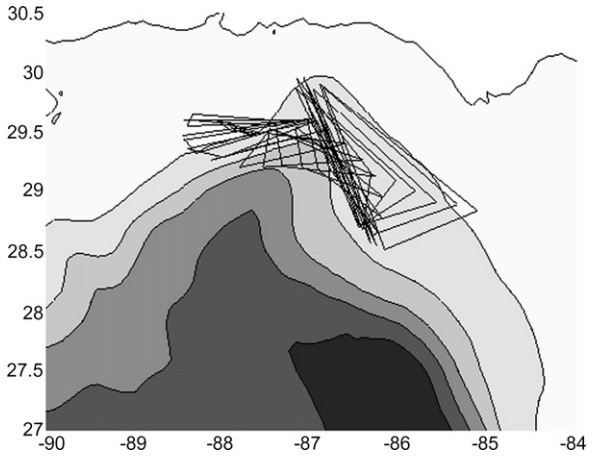


**Fig. 27.** A triplet of drifters in the SCULP experiment. From LaCasce and Ohlmann (2003).

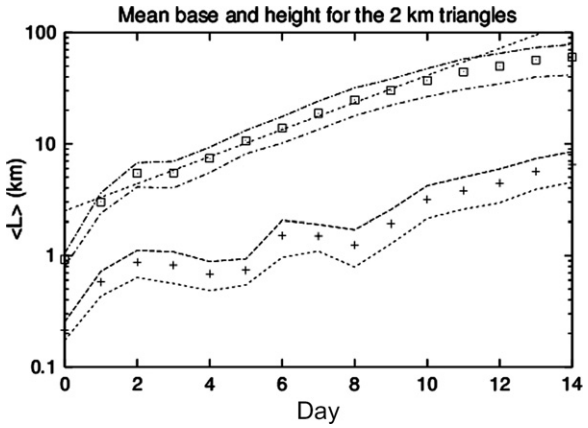


**Fig. 28.** Mean base (defined as the longest leg) and height of 32 triangles from the SCULP experiment. The straight dashed line indicates exponential growth with an e-folding time of 1.8 days. From LaCasce and Ohlmann (2003).

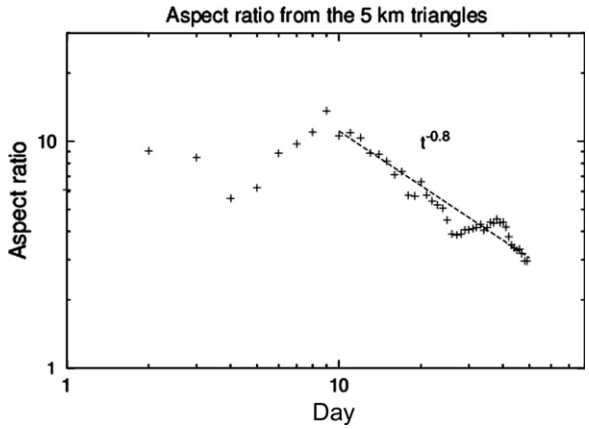


**Fig. 29.** The mean aspect ratio (defined as the base, the longest leg, divided by the height) for the 32 triplets of drifters in the SCULP experiment. From LaCasce and Ohlmann (2003).

although it is not significantly different from 1 km for most of the first 8 days. Thereafter it is clearly growing. However, the latter may signal the shift to the large scale dispersion (note the leg appears to fall off the exponential growth at about the same time). Nevertheless, even if the triangle height were constant, the area is increasing exponentially fast over the initial period.

Molinari and Kirwan (1975) and Fahrbach et al. (1986) also examined the evolution of the areas of clusters of drifters, in the Western Caribbean and the Equatorial Atlantic respectively. The rms drifter separations were comparable to those in SCULP, on the order of a few kilometres. The areas also grew in time (e.g. Fig. 26), and Fahrbach et al. suggested the growth was exponential.

However, this growth in triangle area does not necessarily reflect divergence. Even if the divergence were zero, we could not see the mean triangle height shrink below 1 km, the spatial resolution of the drifter positions. In addition, small scale mixing, due for instance to inertial oscillations, could be preventing a further collapse in the triangle height.

A similar effect is seen at depth. The North Atlantic Tracer Release Experiment (NATRE; Ledwell et al., 1998), in the northeast Atlantic, was one of several such experiments in which a patch of tracer (sulfur hexafluoride) was released on an isopycnal surface and subsequently monitored from a ship. The major result of NATRE was a definitive quantification of the vertical diffusivity in the open ocean. But the lateral spreading reflects the relative dispersion due to the synoptic scale eddy field. The tracer was drawn out into filaments, consistent with sub-deformation scale exponential stretching. These became thinner and thinner until, apparently, small scale mixing limited their further collapse (Sundermeyer and Price, 1998). Such behavior was anticipated in the theoretical work of Garrett (1983).

What happens to a drifter triplet at larger scales? As noted, there are several indications of local relative dispersion at scales greater than the deformation radius (LaCasce and Bower, 2000; Ollitrault et al., 2005; LaCasce and Ohlmann, 2003), so we could ask how such dispersion affects triplets. Triplets have been studied recently in the context of Richardson dispersion (Celani and Vergassola, 2001; Falkovich et al., 2001). Area is not conserved because fluid is mixed in and out of the triangle. One expects the mean square triangle leg to grow at the same rate as the mean pair separation, but theory also suggests the triangles should evolve toward a more equilateral shape. The SCULP triangles are stretched out during the first 10 days, so local dispersion at larger scales should reverse that tendency.

The growth of the rms leg among the SCULP triangles exhibits a power law growth similar to that of the pairs, with an exponent of $n \approx 2.2$ (LaCasce and Ohlmann, 2003). More interestingly, the mean triangle aspect ratio (defined as the base divided by the height) systematically decreases during this period (Fig. 29). So the triangles are indeed shifting toward a more equilateral shape. The aspect ratio exhibits an approximate power law dependence on time, with an exponent of roughly $-1$.

As noted in Section 3.3, some aspects of the late time relative dispersion for the SCULP drifters resemble a Richardson regime while others suggest shear dispersion. The change in aspect ratio is perhaps more consistent with a turbulent cascade. But this issue is certainly not settled and deserves further attention.

## 4. Summary and conclusions

We have examined single and multiple particle statistics applied to ocean data. Single particle studies are the most common; the results of the studies discussed herein can be summarized as follows:

- *Eulerian mean velocities*. By binning drifter velocities geographically, one can map the Eulerian currents. This has been done in many regions, and at different depths. Recent advances include the use of objective analysis and spline-fitting to improve the estimates.
- *Lateral diffusivities*. Diffusivities are estimated from residual velocities. As with the binned means, the diffusivities can be mapped over the regions sampled by the drifters. The results are important for numerical models, particularly when the models do not explicitly resolve eddy transport processes.
- *Stochastic models*. A specifically Lagrangian construct in which synthetic particles are advected, subject to random forcing. Recent models which simulate random accelerations and particle looping can reproduce observed statistics remarkably well.
- *Correlations with other fields*. Correlating drifter velocities or displacements with stationary fields (e.g. topography) can reveal how those fields influence the motion. Correlations with non-stationary fields (e.g. temperature) can be used to estimate eddy-fluxes.
- *PDFs*. Measurements of the velocity probability density functions for both drifters and floats suggest an excess of extreme events over what would be expected for a Gaussian process. This has implications for sub-grid scale modeling, as well as for submerged platforms.
- *Euler–Lagrange relations*. Determining the relation between Eulerian and Lagrangian diffusivities is important if one is to use float-based estimates in models. Recent results suggest converting from one to the other is possible.

Multiple particle dispersion quantifies how tracer spreads. There are fewer such studies than with single particles, but some results are emerging.

- *Sub-deformation dispersion*. There are indications that relative dispersion below the deformation radius is isotropic and increases exponentially in time (Lacorata et al., 2001; LaCasce and Ohlmann, 2003; Ollitrault et al., 2005). As such, the dispersion resembles that seen at similar scales in the stratosphere (Morel and Larcheveque, 1974; Er-el and Peskin, 1981). The cause for the latter is likely non-local straining due to Rossby waves, but the reason for the oceanic dispersion has not been established. If exponential growth is common at these scales, it would aid sub-gridscale mixing parameterizations in numerical models.
- *Dispersion above the deformation radius* is less settled. Some studies suggest Richardson dispersion up to several hundred kilometers (Okubo, 1971; LaCasce and Bower, 2000; LaCasce and Ohlmann, 2003; Ollitrault et al., 2005) while others suggest diffusive spreading (LaCasce and Bower, 2000, in the eastern Atlantic). The situation is similarly unsettled in the stratosphere above the deformation radius. It is most likely the dispersion at these scales is intimately linked to the large scale circulation. Since these scales are resolved by numerical models, the issue could be studied using synthetic floats.
- *Vorticity and divergence estimates*. With a cluster of drifters which are close together and which constitute a polygon with a not-too-large aspect ratio, one can obtain estimates of the vorticity and deformation terms. Divergence is more difficult to resolve, probably because geostrophic velocities are approximately non-divergent.

Thus Lagrangian data has been used profitably to study oceanic dynamics. There are nevertheless a number of outstanding fundamental issues. Our conception of relative dispersion in particular would benefit from more targeted experiments. In most existing data sets, the drifters and floats were deployed alone, necessitating using chance pairs to study relative dispersion. Systematic deployments of pairs and clusters of floats and/or drifters would greatly improve the reliability of the results. Float deployments could also be made in conjunction with tracer releases, so that each data set could compliment the other.

Such experiments would help define the dispersion below and above the deformation radius. As noted earlier, Okubo (1971) deduced Richardson-type dispersion over scales of 10 m to 100 km, while the drifter and float studies suggest exponential growth (LaCasce and Ohlmann, 2003; Ollitrault et al., 2005). The same comments apply for the dispersion at large scales, which is probably influenced by the general circulation. Such experiments would also help sort out differences between surface and sub-surface dispersion, which have been treated essentially interchangeably here. Understanding this is important for using surface data to infer subsurface dispersion.

The dispersion regimes in the ocean could likely be clarified with systematic modeling studies. The study of Huber et al. (2001) revealed regional variations in relative dispersion in the troposphere, and a similar study in the North Atlantic would be useful. The much larger number of particles afforded by a model allows for greater statistical certainty, and this can help determine which measures are robust (e.g. Righi and Strub, 2001; Lumpkin et al., 2002; Bracco et al., 2003; Haza et al., in press). Of course the models cannot capture all aspects, such as the dispersion at small scales, but they would provide a much-needed framework for interpreting the observations.

Lagrangian data is important for studying and modelling the ocean. Lagrangian analyses can produce estimates of the mean velocities and diffusivities in regions where Eulerian sampling is not practical. Eddy heat fluxes are crucially important in climate models, and the best estimates are likely to come from Lagrangian measurements. And with advances in assimilation and the growing number of surface and subsurface observations, Lagrangian data will only become more important in the future.

## Acknowledgements

The present article derives from lectures given at the Summer School "Transport in Geophysical Flows: Ten Years after" in Aosta, Italy in June 2004. The original notes appear in *Transport and Mixing in Geophysical Flows* (Springer-Verlag, 262 pp). Thanks to R. Davis, S. Gille, A. Provenzale, V. Rupolo and three anonymous reviewers for detailed comments on the manuscript, to A. Poje for discussions about the FSLE and to the authors who kindly allowed reproduction of their figures. Dedicated to Dad.

## References

Anikiev, V.V., Zaytsev, O.V., Zaytseva, T.V., Yarosh, V.V., 1985. Experimental investigation of the diffusion parameters in the ocean. Izvestiya Atmospheric and Oceanic Physics 21, 931–934.
Artale, V., Boffetta, G., Celani, A., Cencini, M., Vulpiani, A., 1997. Dispersion of passive tracers in closed basins: beyond the diffusion coefficient. Physics of Fluids 9, 3162–3171.
Aurell, E., Boffetta, G., Crisianti, A., Paladin, G., Vulpiani, A., 1997. Predictability in the large: an extension of the concept of Lyapunov exponent. Journal Physics A: Mathematical General 30, 1–26.
Babiano, A., Basdevant, C., LeRoy, P., Sadourny, R., 1990. Relative dispersion in two-dimensional turbulence. Journal of Fluid Mechanics 214, 535–557.
Batchelor, G.K., 1950. The application of the similarity theory of turbulence to atmospheric diffusion. Quarterly Journal of the Royal Meteorological Society 76, 133–146.
Batchelor, G.K., 1952a. Diffusion in a field of homogeneous turbulence, II; the relative motion of particles. Proceedings of the Cambridge Philosophical Society 48, 345–362.
Batchelor, G.K., 1952b. The effect of homogeneous turbulence on material lines and surfaces. Proceedings of the Royal Society, A 213, 349–366.
Batchelor, G.K., Townsend, A.A., 1953. Turbulent diffusion. Surveys in Mechanics 23, 352–398.
Batchelor, G.K., 1953. The Theory of Homogeneous Turbulence. Cambridge University Press. p. 197.
Bauer, S., Swenson, M.S., Griffa, A., Mariano, A.J., Owens, K., 1998. Eddy-mean flow decomposition and eddy-diffusivity estimates in the tropical Pacific Ocean. 1. Methodology. Journal of Geophysical Research 103, 30,855–30,871.
Bennett, A.F., 1984. Relative dispersion: local and nonlocal dynamics. Journal of Atmospheric Sciences 41, 1881–1886.
Bennett, A.F., 1987. A Lagrangian analysis of turbulent diffusion. Reviews of Geophysics 25 (4), 799–822.
Bennett, A.F., 2006. Lagrangian Fluid Dynamics. Cambridge University Press. p. 286.
Berloff, P.S., McWilliams, J.C., Bracco, A., 2002. Material transport in oceanic gyres. Part I: phenomenology. Journal of Physical Oceanography 32, 764–796.
Berloff, P.S., McWilliams, J.C., 2002. Material transport in oceanic gyres. Part II: hierarchy of stochastic models. Journal of Physical Oceanography 32, 797–830.
Boffetta, G., Celani, A., 2000. Pair dispersion in turbulence. Physica A 280, 1–9.
Borgas, M.S., Fleisch, T.K., Sawford, B.L., 1997. Turbulent dispersion with broken reflectional symmetry. Journal of Fluid Mechanics 332, 141–156.
Bowden, K.F., 1965. Horizontal mixing in the sea due to a shearing current. Journal of Fluid Mechanics 21, 83–95.
Bracco, A., LaCasce, J.H., Provenzale, A., 2000a. Velocity PDFs for oceanic floats. Journal of Physical Oceanography 30, 461–474.
Bracco, A., LaCasce, J.H., Pasquero, C., Provenzale, A., 2000b. The velocity distribution of barotropic turbulence. Physics of Fluids 12, 2478–2488.
Bracco, A., Chassignet, E.P., Garraffo, Z.D., Provenzale, A., 2003. Lagrangian velocity distribution in a high-resolution numerical simulation of the North Atlantic. Journal of Atmospheric and Oceanic Technology 20, 1212–1220.
Bretherton, F.P., Davis, R.E., Fandry, C.B., 1976. A technique for objective analysis and design of oceanographic experiments applied to MODE-73. Deep-Sea Research 23, 559–582.
Brink, K.H., Beardsley, R.C., Niiler, P.P., Abbott, M., Huyer, A., Ramp, S., Stanton, T., Stuart, D., 1991. Statistical properties of near-surface flow in the California Coastal Transition Zone. Journal of Geophysical Research 96 (C8), 14693–14706.
Celani, A., Vergassola, M., 2001. Statistical geometry in scalar turbulence. Physical Review Letters 86, 424–427.
Charney, J., 1971. Geostrophic turbulence. Journal of Atmospheric Sciences 28, 1087–1095.
Cheney, R.E., Richardson, P.L., 1976. Observed decay of a cyclonic Gulf Stream ring. Deep-Sea Research 23, 143–155.

Chin, T.M., Ide, K., Jones, C.K.R.T., Kuznetsov, L., Mariano, A.J., 2007. In: Griffa, A. et al. (Eds.), Lagrangian Analysis and Prediction of Coastal and Ocean Dynamics. Cambridge University Press, pp. 204–230.
Colin de Verdiere, A., 1983. Lagrangian eddy statistics from surface drifters in the eastern North Atlantic. Journal of Marine Research 41, 375–398.
Corrsin, S., 1959. Progress report on some turbulent diffusion research. Advances in Geophysics, vol. 6. Academic Press. pp. 161–162.
D'Agostino, R.B., Stephens, M.A., 1986. Goodness-of-Fit Techniques. Marcel-Dekker, Inc.. p. 576.
Davis, R.E., 1982. On relating Eulerian and Lagrangian velocity statistics: single particles in homogeneous flows. Journal of Fluid Mechanics 114, 1–26.
Davis, R.E., 1983. Oceanic property transport, Lagrangian particle statistics and their prediction. Journal of Marine Research 41, 163–194.
Davis, R.E., 1985. Drifter observations of coastal surface currents during CODE: the statistical and dynamical view. Journal of Geophysical Research 90, 4756–4772.
Davis, R.E., 1987. Modelling eddy transport of passive tracers. Journal of Marine Research 45, 635–666.
Davis, R.E., 1990. Lagrangian ocean studies. Annual Review of Fluid Mechanics 23, 43–64.
Davis, R.E., 1991. Observing the general circulation with floats. Deep-Sea Research 38 (Suppl.), S531–S571.
Davis, R.E., 1998. Preliminary results from directly measuring mid-depth circulation in the Tropical and South Pacific. Journal of Geophysical Research 103, 24619–24639.
Davis, R.E., Regier, L.A., Dufour, J., Webb, D.C., 1992. The autonomous Lagrangian circulation explorer (ALACE). Journal of Atmospheric and Oceanic Technology 9, 264–285.
Er-el, J., Peskin, R., 1981. Relative diffusion of constant-level balloons in the Southern hemisphere. Journal of Atmospheric Sciences 38, 2264–2274.
Fahrbach, E., Brockmann, C., Meincke, J., 1986. Horizontal mixing in the Atlantic equatorial undercurrent estimated from drifting buoy clusters. Journal of Geophysical Research 91, 10557–10565.
Falco, P., Griffa, A., Poulain, P., Zambianchi, E., 2000. Transport properties in the Adriatic Sea as deduced from drifter data. Journal of Physical Oceanography 30, 2055–2071.
Falkovich, G., Gawedzki, K., Vergassola, M., 2001. Particles and fields in fluid turbulence. Reviews of Modern Physics 73 (4), 913–975.
Ferrari, R., Manfroi, A.J., Young, W.R., 2001. Strongly and weakly self-similar diffusion. Physica D 154, 111–137.
Figueroa, H.A., Olson, D.B., 1989. Eddy resolution versus eddy diffusion in a double gyre GCM. Part I: the Lagrangian and Eulerian description. Journal of Physical Oceanography 24, 371–386.
Fischer, J., Schott, F.A., 2002. Labrador Sea water tracked by profiling floats—from the boundary current into the open North Atlantic. Journal of Physical Oceanography 32, 573–584.
Flierl, G.R., 1981. Particle motions in large-amplitude wave fields. Geophysical and Astrophysical Fluid Dynamics 18, 39–74.
Fratantoni, D.M., 2001. North Atlantic surface circulation during the 1990s observed with satellite-tracked drifters. Journal of Geophysical Research 106, 22067–22093.
Freeland, H.J., Rhines, P.B., Rossby, T., 1975. Statistical observations of the trajectories of neutrally buoyant floats in the North Atlantic. Journal of Marine Research 33, 383–404.
Frenkiel, F.N., Katz, I., 1956. Studies of small-sale turbulent diffusion in the atmosphere. Joural of Meteorology 13, 388–394.
Gage, K.S., Nastrom, G.D., 1986. Theoretical interpretation of atmospheric spectra of wind and temperature observed by commercial aircraft during GASP. Journal of Atmospheric Sciences 43, 729–740.
Gardner, C.W., 2004. Handbook of Stochastic Methods: for Physics, Chemistry and the Natural Sciences. Springer. p. 415.
Garrett, C., 1983. On the initial streakiness of a dispersing tracer in two- and three-dimensional turbulence. Dynamics of Atmospheres and Oceans 7, 265–277.
Gifford, F., 1957. Relative atmospheric diffusion of smoke puffs. Journal of Meteorology 14, 410–414.
Gille, S., 2003. Float observations of the Southern Ocean: part 1, estimating mean fields, bottom velocities, and topographic steering. Journal of Physical Oceanography 33, 1167–1181.
Gould, W.J., 2005. From swallow floats to Argo2014the development of neutrally buoyant floats. Deep-Sea Research II 52, 529–543.
Griffa, A., Owens, K., Piterbarg, L., Rozovskii, B., 1995. Estimates of turbulence parameters from Lagrangian data using a stochastic particle model. Journal of Marine Research 53, 371–401.
Haza, A.C., Poje, A.C., Özgökmen, T.M. and Miller, P. in press. Relative dispersion from a high-resolution coastal model of the Adriatic Sea. Ocean Modelling.
Hogg, N.C., Owens, W.B., 1999. Direct measurements of the deep circulation within the Brazil Basin. Deep-Sea Research 46, 335–353.
Huber, M., McWilliams, J.C., Ghil, M., 2001. A climatology of turbulent dispersion in the troposphere. Journal of Atmospheric Sciences 58, 2377–2394.
Isern-Fontanet, J., Garcia-Ladona, E., Font, J., Garcia-Olivares, A., 2006. Non-Gaussian velocity probability density functions: an altimetric perspective of the Mediterranean sea. Journal of Physical Oceanography 36, 2153–2164.
Jakobsen, P.K., Rikergaard, M.H., Quadfasel, D., Schmith, T., Hughes, C.W., 2003. The near surface circulation in the Northern North Atlantic as inferred from Lagrangian drifters: variability from the mesoscale to interannual. Journal of Geophysical Research 108. doi:10.1029/2002JC001554.
Jimenez, J., 1996. Probability densities in two-dimensional turbulence. Journal of Fluid Mechanics 313, 223–240.
Jullian, P., Massman, W., Levanon, N., 1977. The TWERLE experiment. Bulletin of the American Meteorological Socitey 58, 936–948.
Kampé de Fériet, J., 1939. Les fonctions aléatoires stationnaires et la théorie statistique de la turbulence homogéne. Annales de la Societe Scientifique de Bruxelles 59, 145–194.
Kirwan, A.D., McNally, G.J., Reyna, E., Merrell, W.J., 1978. The near-surface circulation of the eastern North Pacific. Journal of Physical Oceanography 8, 937–945.
Kolmogorov, A.N., 1941. The local structure of turbulence in incompressible viscous fluid for very large Ryeynolds number. Doklady Akademii Nauk SSSR 30, 9–13.
Kraichnan, R.H., 1966. Dispersion of particle pairs in homogeneous turbulence. Physics of Fluids 9, 1937–1943.
Kraichnan, R.H., 1967. Inertial ranges of two dimensional turbulence. Physics of Fluids 10, 1417–1423.
Krauss, W., Böning, C.W., 1987. Lagrangian properties of eddy fields in the northern North Atlantic as deduced from satellite-tracked buoys. Journal of Marine Research 45, 259–291.
Kuznetsov, L., Toner, M., Kirwan, A.D., Jones, C.K.R.T., Kantha Jr., L.H., Choi, J., 2002. The loop current and adjacent rings delineated by Lagrangian analysis of the near-surface flow. Journal of Marine Research 60, 405–429.
LaCasce, J.H., 2000. Floats and $f/H$. Journal of Marine Research 58, 61–95.
LaCasce, J.H., 2005. On the Eulerian and Lagrangian velocity distributions in the North Atlantic. Journal of Physical Oceanography 35, 2327–2336.
LaCasce, J.H., Speer, K.G., 1999. Lagrangian statistics in unforced barotropic flows. Journal of Marine Research 57, 245–274.
LaCasce, J.H., Bower, A., 2000. Relative dispersion in the subsurface North Atlantic. Journal of Marine Research 58, 863–894.
LaCasce, J.H., Ohlmann, C., 2003. Relative dispersion at the surface of the Gulf of Mexico. Journal of Marine Research 61, 285–312.
Lacorata, G., Aurell, E., Vulpiani, A., 2001. Drifter dispersion in the Adriatic Sea: Lagrangian data and chaotic model. Annales Geophysicae 19, 121–129.
Lacorata, G., Aurell, E., Legras, B., Vulpiani, A., 2004. Evidence for a $\kappa^{-5/3}$ spectrum from the EOLE Lagrangian balloons in the low stratosphere. Journal of Atmospheric Sciences 61, 2936–2942.
Lavender, K.A., Davis, R.E., Owens, W.B., 2000. Mid-depth recirculation observed in the interior Labrador and Irminger seas by direct velocity measurements. Nature 407, 66–69.
Lavender, K.A., Davis, R.E., Owens, W.B., 2005. The mid-depth circulation of the subpolar North Atlantic Ocean as measured by subsurface floats. Deep-Sea Research 52A, 767–785.
Ledwell, J.R., Watson, A.J., Law, C.S., 1998. Mixing of a tracer in the pycnocline. Journal of Geophysical Research 103, 21499–21529.
Lichtenberg, A.J., Lieberman, M.A., 1992. Regular and Chaotic Dynamics. Springer-Verlag. p. 714.
Lin, J.-T., 1972. Relative dispersion in the enstrophy-cascading inertial range of homogeneous two-dimensional turbulence. Journal of Atmospheric Sciences 29, 394–395.
Lozier, M.S., Pratt, L.J., Rogerson, A.M., Miller, P.D., 1997. Exchange geometry revealed by float trajectories in the Gulf Stream. Journal of Physical Oceanography 27, 2327–2341.
Lumpkin, R., Flament, P., 2001. Lagrangian statistics in the central North Pacific. Journal of Marine Systems 29, 141–155.
Lumpkin, R., Treguier, A.-M., Speer, K., 2002. Lagrangian eddy scales in the northern Atlantic Ocean. Journal of Physical Oceanography 32, 2425–2440.
Lumpkin, R., Pazos, M., 2007. Measuring surface currents with SVP drifters. In: Griffa, A. et al. (Eds.), Lagrangian Analysis and Prediction of Coastal and Ocean Dynamics. Cambridge University Press, pp. 39–67.
Lundgren, T.S., 1981. Turbulent pair dispersion and scalar diffusion. Journal of Fluid Mechanics 111, 27–57.
Mariano, A.J., Rossby, H.T., 1989. The Lagrangian potential vorticity balance during POLYMODE. Journal of Physical Oceanography 19, 927–939.
Maurizi, A., Griffa, A., Poulain, P.M., Tampieri, F., 2004. Lagrangian turbulence in the Adriatic Sea as computed from drifter data: effects of inhomogeneity and nonstationarity. Journal of Geophysical Research 109 (C4). C0401010.1029/2003JC002119.
Mauritzen, C., 1996. Production of dense overflow waters feeding the North Atlantic across the Greenland–Scotland Ridge. Part 1: evidence for a revised circulation scheme. Deep-Sea Research 43, 769–806.
McWilliams, J.C., Brown, E.D., Bryden, H.L., Ebbesmeyer, C.C., Elliot, B.A., Heinmiller, R.H., Lien Hua, B., Leaman, K.D., Lindstrom, E.J., Luyten, J.R., McDowell, S.E., Breckner Owens, W., Perkins, H., Price, J.F., Regier, L., Riser, S.C., Rossby, H.T., Sanford, T.B., Shen, C.Y., Taft, B.A., van Leer, J.C., 1983. The local dynamics of eddies in the western North Atlantic. In: Eddies in Marine Science. Springer-Verlag, p. 609.
Middleton, J., 1985. Drifter spectra and diffusivities. Journal of Marine Research 43, 37–55.
Molcard, A., Özgökmen, T.M., Griffa, A., Piterbarg, L.I., Chin, T.M., 2007. Lagrangian data assimilatio in ocean general circulation models. In: Griffa, A. et al. (Eds.), Lagrangian Analysis and Prediction of Coastal and Ocean Dynamics. Cambridge University Press, pp. 172–203.
Molinari, R., Kirwan Jr., A.D., 1975. Calculations of differential kinematic properties from Lagrangian observations in the Western Caribbean Sea. Journal of Physical Oceanography 5, 483–491.

Monin, A.S., Yaglom, A.M., 2007. Statistical Fluid Mechanics: Mechanics of Turbulence, vol. I. Dover. 784 pp.
Morel, P., Bandeen, W., 1973. The EOLE experiment, early results and current objectives. Bulletin of the American Meteorological Socitey 54, 298–306.
Morel, P., Larcheveque, M., 1974. Relative dispersion of constant-level balloons in the 200 mb general circulation. Journal of Atmospheric Sciences 31, 2189–2196.
Niiler, P.P., Poulain, P.-M., Haury, L.R., 1989. Synoptic three-dimensional circulation in an onshore-flowing filament of the California Current. Deep-Sea Research 36, 385–405.
Niiler, P.P., Sybrandy, A.S., Bi, K., Poulain, P.M., Bitterman, D., 1995. Measurements of the water-following capability of holey-sock and TRISTAR drifters. Deep-Sea Research I 42, 1951–1964.
Obhukov, A.M., 1941. Energy distribution in the spectrum of turbulent flow. Izvestiya Akademii Nauk SSSR Seriya Geograficheskaya I Geofizichaskaya 5, 453–466.
O'Dwyer, J., Williams, R.G., LaCasce, J.H., Speer, K.G., 2000. Does the PV distribution constrain the spreading of floats in the N. Atlantic? Journal of Physical Oceanography 30, 721–732.
Ohlmann, J.C., White, P.F., Sybrandy, A.L., Niiler, P.P., 2005. GPS-cellular drifter technology for coastal ocean observing systems. Journal of Atmospheric and Oceanic Technology 22, 1381–1388.
Ohlmann, J.C., Niiler, P.P., 2005. A two-dimensional response to a tropical storm on the Gulf of Mexico shelf. Progress in Oceanography 29, 87–99.
Okubo, A., 1971. Oceanic diffusion diagrams. Deep-Sea Research 18, 789–802.
Okubo, A., Ebbesmeyer, C., 1976. Determination of vorticity, divergence and deformation rates from analysis of drogue observations. Deep-Sea Research 23, 349–352.
Okubo, A., Ebbesmeyer, C.C., Helseth, J.M., 1976. Determination of Langrangian deformations from analysis of current followers. Journal of Physical Oceanography 6, 524–527.
Ollitrault, M., Gabillet, C., Colin de Verdiere, A., 2005. Open ocean regimes of relative dispersion. Journal of Fluid Mechanics 533, 381–407.
Owens, W.B., 1991. A statistical description of the mean circulation and eddy variability in the northwestern North Atlantic using SOFAR floats. Progress in Oceanography 28, 257–303.
Paduan, J.D., Niiler, P.P., 1990. A Langrangian description of motion in northern California coastal transition filaments. Journal of Geophysical Research 95, 18095–18109.
Pasquero, C., Provenzale, A., Babiano, A., 2001. Parameterization of dispersion in two-dimensional turbulence. Journal of Fluid Mechanics 439, 279–303.
Poulain, P.M., Niiler, P.P., 1989. Statistical analysis of the surface circulation in the California current system using satellite-tracked drifters. Journal of Physical Oceanography 19, 1588–1603.
Poulain, P.M., Warn-Varnas, A., Niiler, P.P., 1996. Near-surface circulation of the Nordic Seas as measured by Lagrangian drifters. Journal of Geophysical Research 101, 18237–18258.
Price, J.F., Rossby, T., 1982. Observations of a barotropic planetary wave in the western North Atlantic. Journal of Marine Research 40, 543–558.
Reynolds, A.M., 2003. Third-order Lagrangian stochastic modeling. Physics of Fluids 15, 2773–2777.
Richardson, L.F., 1926. Atmospheric diffusion on a distance–neighbour graph. Proceedings of the Royal Society of London, Series A 110, 709–737.
Richardson, L.F., Stommel, H., 1948. Note on eddy diffusion in the sea. Journal of Meteorology 5 (5), 38–40.
Richardson, P.L., 1983. Eddy kinetic energy in the North Atlantic from surface drifters. Journal of Geophysical Research 88 (C7), 4355–4367.
Richardson, P.L., 1993. A census of eddies observed in North Atlantic SOFAR float data. Progress in Oceanography 31, 1–50.
Richardson, P.L., Walsh, D., Armi, L., Schroder, M., Price, J.F., 1989. Tracking three Meddies with SOFAR floats. Journal of Physical Oceanography 19, 371–383.
Riley, J.J., Corrsin, S., 1974. The relation of turbulent diffusivities to Lagrangian velocity statistics for the simplest shear flow. Journal of Geophysical Research 79, 1768–1771.
Righi, D.D., Strub, T., 2001. The use of simulated drifters to estimate vorticity. Journal of Marine Systems 29, 125–140.
Rodean, H., 1996. Stochastic Lagrangian models of turbulent diffusion. Meteorological Monographs 26 (48). American Meteorological Society.
Rogerson, A.M., Miller, P.D., Pratt, L.J., Jones, C., 1999. Lagrangian motion and fluid exchange in a barotropic meandering jet. Journal of Physical Oceanography 29, 2635–2655.
Rossby, T., Webb, D., 1970. Observing abyssal motions by tracking Swallow floats in the SOFAR channel. Deep-Sea Research 17, 359–365.
Rossby, H.T., Levine, E.R., Connors, D.N., 1985. The isopycnal swallow float—a simple device for tracking water parcels in the ocean. Progress in Oceanography 14, 511–525.
Rossby, H.T., Dorson, D., Fontaine, J., 1986. The RAFOS system. Journal of Atmospheric and Oceanic Technology 3, 672–679.
Rossby, H.T., 2007. Evolution of Lagrangian methods in oceanography. In: Griffa, A. et al. (Eds.), Lagrangian Analysis and Prediction of Coastal and Ocean Dynamics. Cambridge University Press, pp. 1–38.
Rupolo, V., Hua, B.L., Provenzale, A., Artale, V., 1996. Lagrangian velocity spectra at 700 m in the western North Atlantic. Journal of Physical Oceanography 26, 1591–1607.
Rupolo, V., 2007. A Lagrangian-based approach for determining trajectories taxonomy and turbulence regimes. Journal of Physical Oceanography 37, 1584–1609.
Salmon, R., 1980. Baroclinic instability and geostrophic turbulence. Geophysical and Astrophysical Fluid Dynamics 10, 25–52.
Saucier, W.J., 1955. Principles of Meterorological Analysis. Univ. of Chicago Press. p. 438.
Sawford, B.L., 1991. Reynolds number effects in Lagrangian stochastic models of turbulent dispersion. Physics of Fluids A 3, 1577–1586.
Sawford, B.L., 1999. Rotation of trajectories in Lagrangian stochastic models of turbulent dispersion. Boundary Layer Meteorology 93, 411–424.
Sawford, B.L., 2001. Turbulent relative dispersion. Annual Review of Fluid Mechanics 33, 289–317.
Schumacher, J., Eckhardt, B., 2002. Clustering dynamics of Lagrangian tracers in free-surface flows. Physical Review E 66, 017303.
Scott, R.G., Wang, F., 2005. Direct evidence of an oceanic inverse kinetic energy cascade from satellite altimetry. Journal of Physical Oceanography 35, 1650–1666.
Shepherd, T.G., Koshyk, J.N., Ngan, K., 2000. On the nature of large-scale mixing in the stratosphere and mesosphere. Journal of Geophysical Research 105, 12433–12446.
Solomon, T.H., Weeks, E.R., Swinney, H.L., 1993. Observation of anomalous diffusion and Levy flights in a two-dimensional rotating flow. Physical Review Letters 71 (24), 3975–3978.
Spall, M.A., Richardson, P.L., Price, J., 1993. Advection and eddy mixing in the Mediterranean salt tongue. Journal of Marine Research 51, 797–818.
Stammer, D., 1997. Global characteristics of ocean variability estimated from regional TOPEX/POSEIDON altimeter measurements. Journal of Physical Oceanography 27, 1743–1769.
Stommel, H.M., 1949. Horizontal diffusion due to oceanic turbulence. Journal of Marine Research 8, 199–225.
Sundermeyer, M.A., Price, J.F., 1998. Lateral mixing and the North Atlantic tracer release experiment: observations and numerical simulations of Lagrangian particles and a passive tracer. Journal of Geophysical Research 103, 21481–21497.
Sullivan, P.J., 1971. Some data on the distance–neighbour function for relative diffusion. Journal of Fluid Mechanics 47, 601–607.
Swallow, J.C., Worthington, L.V., 1957. Measurements of deep currents in the western North Atlantic. Nature 179, 1183–1184.
Swallow, J.C., 1971. The Aries current measurements in the Western North Atlantic. Philosophical Transactions of the Royal Society of London 270, 451–460.
Swenson, M.S., Niiler, P.P., 1996. Statistical analysis of the surface circulation of the California Current. Journal of Geophysical Research 101, 22631–22645.
Swenson, M.S., Niiler, P.P., Brink, K.H., Abbott, M.R., 1992. Drifter observations of a cold filament off Point Arena, California. Journal of Geophysical Research 97, 3593–3610.
Sybrandy, A.L. and Niiler, P.P. 1992. WOCE/TOGA Lagrangian drfiter construction manual. WOCE Rep. 63, SIO Ref. 91/6. Scripps Institution of Oceanography, pp. 58.
Taylor, G.I., 1921. Diffusion by continuous movements. Proceedings of the London Mathematical Society 20, 196–212.
Taylor, G.I., 1938. The spectrum of turbulence. Proceedings of the Royal Society, A 64, 476–490.
Tennekes, H., Lumley, J.L., 1972. A First Course in Turbulence. MIT Press. p. 300.
Thiffeault, J.-L., 2005. Measuring topoglogical chaos. Phyical. Review Letters 94 (8), 084502.
Thomson, D.J., 1987. Crieria for the selection of stochastic models of particle trajetories in turbulent flows. Journal of Fluid Mechanics 180, 529–556.
Veneziani, M., Griffa, A., Reynolds, A.M., Garraffo, Z.D., Chassignet, E.P., 2005. Parameterizations of Lagrangian spin statistics and particle dispersion in the presence of coherent vortices. Journal of Marine Research 63 (6), 1057–1083.
Veneziani, M., Griffa, A., Reynolds, A.M., Mariano, A.J., 2004. Oceanic turbulence and stochastic models from subsurface Lagrangian data for the North-West Atlantic Ocean. Journal of Physical Oceanography 34, 1884–1906.
Weiss, J.B., Provenzale, A., McWilliams, J.C., 1998. Lagrangian dynamics in high-dimensional point vortex systems. Physics of Fluids 10, 1929–1941.
Wiggins, S., 2005. The dynamical systems approach to Lagrangian transport in oceanic flows. Annual Review of Fluid Mechanics 37, 295–328.
Wilson, J.D., Sawford, B.L., 1996. Review of Lagrangian stochastic models for trajectories in the turbulent atmosphere. Boundary Layer Meteorology 78, 191–210.
Young, W.R., 1999. Lectures on Stirring and Mixing. Woods Hole Summer Program in Geophysical Fluid Dynamics. Available from: <www-pord.ucsd.edu/wryoung/>.
Zambianchi, E., Griffa, A., 1994. Effects of finite scales of turbulence on dispersion estimates. Journal of Marine Research 52, 129–148.
Zang, X., Wunsch, C., 2001. Spectral description of low-frequency oceanic variability. Journal of Physical Oceanography 31, 3073–3095.
Zhang, H.M., Prater, M.D., Rossby, T., 2001. Isopycnal Lagrangian statistics from North Atlantic Current RAFOS float observations. Journal of Geophysical Research 106, 13,817–13,836.
Zhurbas, V., Oh, I.S., 2004. Drifter-derived maps of lateral diffusivity in the Pacific and Atlantic Oceans in relations to surface circulation patterns. Journal of Geophysical Research 109, C05015.